AD-A190 105 THE EFFECTS OF TIME-DEPENDENT WINDS AND OCEAN EDDIES ON ICE MOTION IN A MARGINAL ICE ZONE(U) NAVAL POSTGRADUATE SCHOOL MONTEREY CA J L BARKER DEC 87 1/1

UNCLASSIFIED F/G 8/12 NL

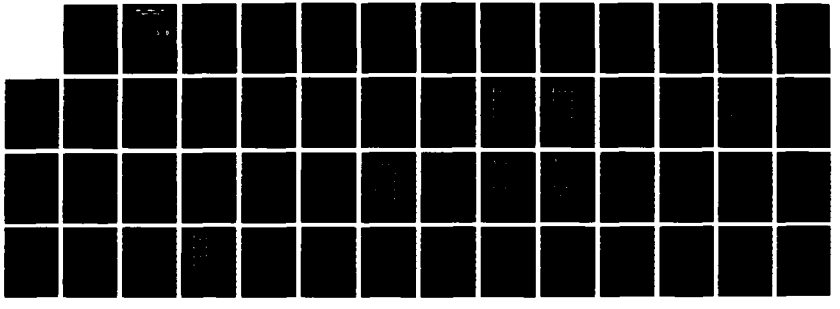

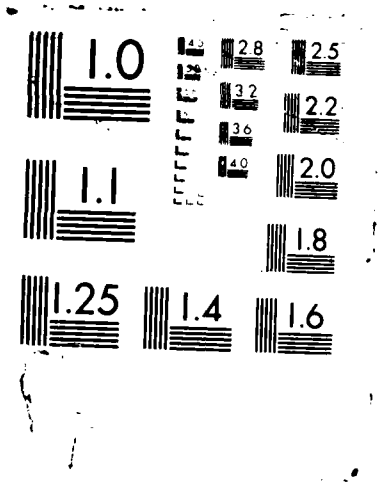
1.0
1.1
1.25
1.4
1.6
1.8
2.0
2.2
2.5
2.8
3.2
3.6
4.0

NAVAL POSTGRADUATE SCHOOL
Monterey, California

THESIS

THE EFFECTS OF TIME-DEPENDENT WINDS
AND OCEAN EDDIES ON ICE MOTION
IN A MARGINAL ICE ZONE

by

Jeffrey L. Barker

December 1987

Thesis Advisor D.C. Smith IV

SECURITY CLASSIFICATION OF THIS PAGE

REPORT DOCUMENTATION PAGE

1a REPORT SECURITY CLASSIFICATION UNCLASSIFIED	1b RESTRICTIVE MARKINGS
2a SECURITY CLASSIFICATION AUTHORITY	3 DISTRIBUTION/AVAILABILITY OF REPORT Approved for public release; distribution is unlimited.
2b DECLASSIFICATION/DOWNGRADING SCHEDULE	
4 PERFORMING ORGANIZATION REPORT NUMBER(S)	5 MONITORING ORGANIZATION REPORT NUMBER(S)
6a NAME OF PERFORMING ORGANIZATION Naval Postgraduate School 6b OFFICE SYMBOL (If applicable) 35	7a NAME OF MONITORING ORGANIZATION Naval Postgraduate School
6c ADDRESS (City, State, and ZIP Code) Monterey, CA 93943-5000	7b ADDRESS (City, State, and ZIP Code) Monterey, CA 93943-5000
8a NAME OF FUNDING/SPONSORING ORGANIZATION 8b OFFICE SYMBOL (If applicable)	9 PROCUREMENT INSTRUMENT IDENTIFICATION NUMBER
8c ADDRESS (City, State, and ZIP Code)	10 SOURCE OF FUNDING NUMBERS PROGRAM ELEMENT NO / PROJECT NO / TASK NO / WORK UNIT ACCESSION NO

11 TITLE (Include Security Classification)
THE EFFECTS OF TIME-DEPENDENT WINDS AND OCEAN EDDIES ON ICE MOTION IN A MARGINAL ICE ZONE

12 PERSONAL AUTHOR(S)
BARKER, Jeffrey L.

13a TYPE OF REPORT	13b TIME COVERED	14 DATE OF REPORT (Year, Month, Day)	15 PAGE COUNT
Master's Thesis	FROM _____ TO _____	1987 December	53

16 SUPPLEMENTARY NOTATION

17 COSATI CODES			18 SUBJECT TERMS (Continue on reverse if necessary and identify by block number)
FIELD	GROUP	SUB-GROUP	MARGINAL ICE ZONE, EAST GREENLAND CURRENT, MESOSCALE EDDIES, NUMERICAL SIMULATIONS

19 ABSTRACT (Continue on reverse if necessary and identify by block number)

Observations made during the MIZEX program indicate the presence of mesoscale eddies in the ocean front at the marginal ice edge in the East Greenland Current. The eddies ranged in scale from 5 to 80 km. Barotropic and baroclinic instability may be the physical mechanisms responsible for the existance of such eddies. The observations also indicate transient wind reversals (3-10 m/s) with a frequency of several days. Here the effect of time-dependent winds and ocean eddies on ice motion in a marginal ice zone is studied. Results are obtained with a two-layer, nonlinear, primitive equation ocean model and a coupled free-drift ice model. The results indicate that ocean eddy signature in the ice edge is sensitive to cross-ice-edge motion induced by the winds and is shown to be dependent on magnitude, direction, and duration of the wind.

20 DISTRIBUTION/AVAILABILITY OF ABSTRACT	21 ABSTRACT SECURITY CLASSIFICATION	
☒ UNCLASSIFIED/UNLIMITED ☐ SAME AS RPT ☐ DTIC USERS	UNCLASSIFIED	
22a NAME OF RESPONSIBLE INDIVIDUAL David Smith	22b TELEPHONE (Include Area Code) (408) 646-3350	22c OFFICE SYMBOL Code 68Si

DD FORM 1473, 84 MAR — 83 APR edition may be used until exhausted. All other editions are obsolete.

SECURITY CLASSIFICATION OF THIS PAGE

Approved for public release; distribution is unlimited.

The Effects of Time-Dependent Winds and Ocean Eddies on Ice Motion in a Marginal Ice Zone

by

Jeffrey L. Barker
Lieutenant Commander, United States Navy
B.S., Georgia Institute of Technology, 1976

Submitted in partial fulfillment of the
requirements for the degree of

MASTER OF SCIENCE IN METEOROLOGY AND OCEANOGRAPHY

from the

NAVAL POSTGRADUATE SCHOOL
December 1987

Author: Jeffrey L. Barker
Jeffrey L. Barker

Approved by: David C. Smith IV
D.C. Smith IV, Thesis Advisor

A.J. Semtner
A.J. Semtner, Second Reader

C.A. Collins
C.A. Collins, Chairman,
Department of Oceanography

G.E. Schacher
Gordon E. Schacher,
Dean of Science and Engineering

ABSTRACT

Observations made during the MIZEX program indicate the presence of mesoscale eddies in the ocean front at the marginal ice edge in the East Greenland Current. The eddies ranged in scale from 5 to 80 km. Barotropic and baroclinic instability may be the physical mechanisms responsible for the existance of such eddies. The observations also indicate transient wind reversals (3-10 m s) with a frequency of several days. Here the effect of time-dependent winds and ocean eddies on ice motion in a marginal ice zone is studied. Results are obtained with a two-layer, nonlinear, primitive equation ocean model and a coupled free-drift ice model. The results indicate that ocean eddy signature in the ice edge is sensitive to cross-ice-edge motion induced by the winds and is shown to be dependent on magnitude, direction, and duration of the wind.

TABLE OF CONTENTS

LIST OF TABLES

LIST OF FIGURES

I. INTRODUCTION

A. THE MARGINAL ICE ZONE AND THE EAST GREENLAND CURRENT

The marginal ice zone is a region where complex atmospheric and oceanic physical processes affect the distribution of ice between the pack ice and the open ocean. In recent years the marginal ice zone (MIZ) in the region of the East Greenland Current has been extensively investigated during Marginal Ice Zone Experiments. The East Greenland Current is arctic (polar) water flowing southward along the east coast of Greenland, over the 200 m deep and 200 km wide continental shelf, and then continuing to flow southward over deeper (4000 m) water (Wadhams *et al.*, 1979). The boundary formed by the arctic water of the East Greenland Current and the Atlantic water is a potentially unstable ocean front. Figure 1.1 shows the location of the East Greenland Current and the mean ice edge.

The study of stability of ocean fronts has been done in the laboratory as well as in numerical experiments. Griffiths and Linden (1981) examined stability characteristics of density driven fronts in rotating tank experiments. Their experiments indicate that the type of instability (barotropic or baroclinic) associated with a given flow field is dependent upon the length scale. In general, if the length scale L of the mean flow is larger than the local internal Rossby radius of deformation (R_d), then the resulting instability is baroclinic. Where the length scale is comparable to R_d, the instability is more likely to be barotropic. The width scale of the East Greenland Current is on the order of 200 km, much greater than the local R_d (8 km), suggesting baroclinic instablity (Griffiths and Linden, 1981). The observed 50 km length scales of some of the eddies (Wadhams and Squire, 1983) appear to be consistent with these considerations. The mesoscale ice edge frontal eddies observed by Johannessen *et al.* (1983) had a length scale comparable to the local internal Rossby radius; therefore, from the above considerations, these mesoscale eddies would be the result of barotropic instability.

B. EDDIES IN THE EAST GREENLAND CURRENT REGION

From an observational standpoint, eddies in the MIZ have only recently been documented. These eddies have been observed to have scales ranging from 5 to 80 km. There are five possible sources for the eddies of the East Greenland Current region:

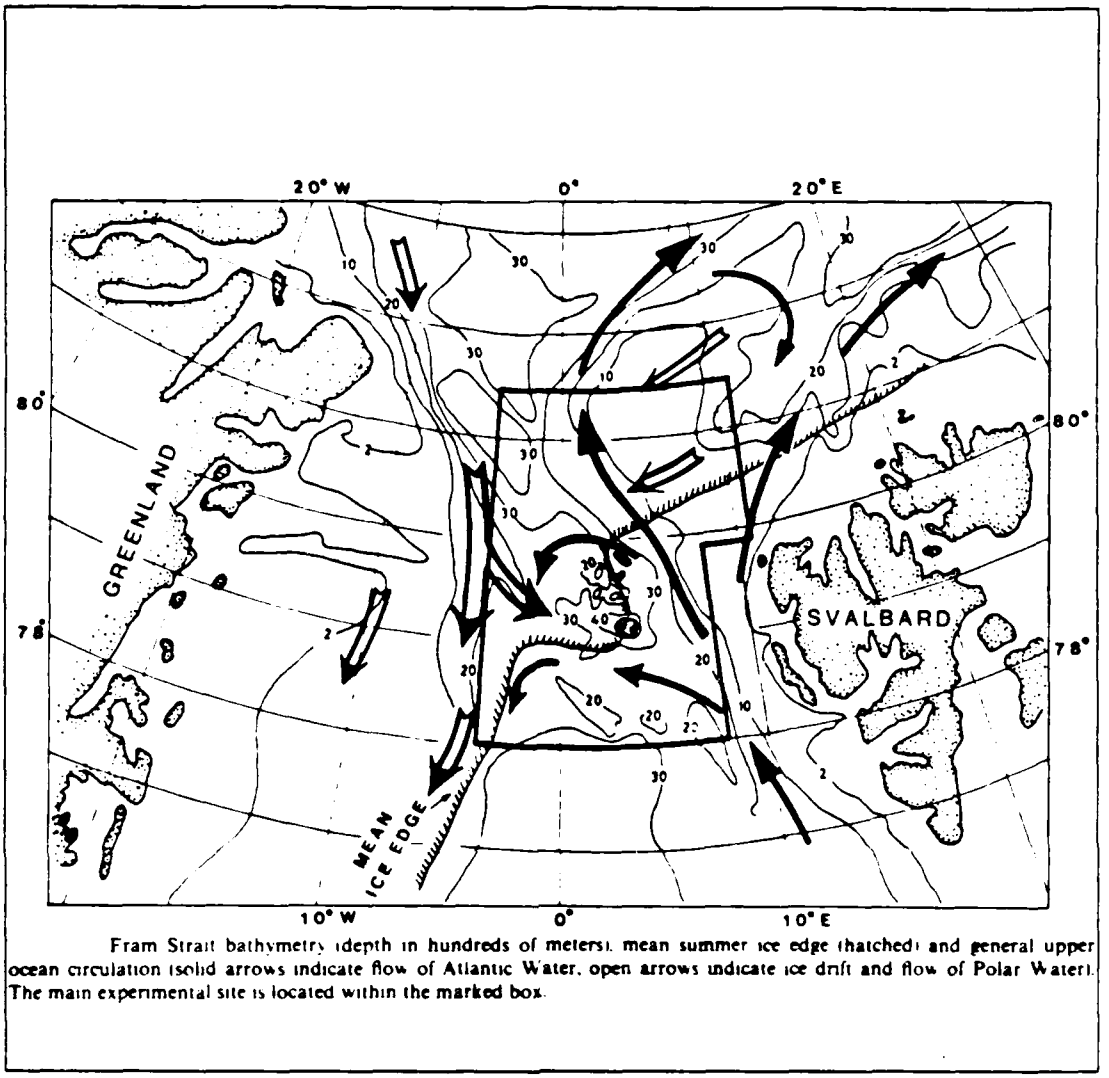

Fram Strait bathymetry (depth in hundreds of meters), mean summer ice edge (hatched) and general upper ocean circulation (solid arrows indicate flow of Atlantic Water, open arrows indicate ice drift and flow of Polar Water). The main experimental site is located within the marked box.

Figure 1.1 Ice-Edge Oceanic Front (from Johannessen *et al.*, 1987).

(1) Barotropic instability was suggested by Johannessen *et al.* (1983) as being responsible for the formation of small-scale eddies; (2) Baroclinic instability is largely responsible for the larger-scale eddies (Griffiths and Linden, 1981); (3) Current-topography interaction may cause eddy formation (Smith *et al.*, 1984); (4) Open ocean eddies present in Atlantic water may be advected toward the ice edge, leading to interaction that can develop into ice-edge eddies (Johannessen *et al.*, 1987); and (5) Ice edge air-sea interaction may cause eddies to form (Røed and O'Brien, 1983; Häkkinen, 1986a, b).

C. MESOSCALE EDDIES

Studies of small-scale (5 to 15 km) eddies observed in conjunction with the ice edge front over deep water (Johannessen *et al.*, 1983 and Johannessen *et al.*, 1987) have significantly increased the knowledge of the structure of mesoscale eddies. The front was observed to have velocities of approximately 10 cm s (with little vertical shear) and a width scale of 10 km. Observations found several mesoscale eddies with length scales ranging from 5 to 15 km associated with the front. Like the front, these associated eddies also exhibited little vertical shear. Based on considerations from theory and laboratory experiments discussed above, Johannessen *et al.* (1983) reasoned that the eddies most likely resulted from barotropic instability of the oceanic front. Johannessen *et al.* (1987) also established that eddies and meanders are the dominant features along the ice edge under moderate wind conditions. Mesoscale eddies are the focus of this study.

D. WIND-FORCED STUDIES

Numerous studies of wind driven ocean motion in the marginal ice zone have been conducted since 1980. Initially these were two-dimensional cross-ice edge examinations of upwelling and downwelling produced by along-ice edge winds (Røed and O'Brien, 1983; Häkkinen, 1986a). Because the coupling is stronger under ice, Ekman transport is larger under ice. Røed and O'Brien (1983) describe the relationship between the wind and the ice edge as " . . . winds which blow along the ice edge and to the left when facing the ice which favors upwelling." Häkkinen (1986b) also showed that along ice edge, 10 m s winds produce upwelling (downwelling) when the ice edge is to the right (left) of wind direction.

Recently, Smith *et al.* (1987) have studied the effect of along-ice edge winds on existing ocean eddies. Their results show that for constant 10 m s winds, the ice responds largely to the wind and, to a lesser extent, the ocean eddy. They also find, however, that upper ocean anticyclones (cyclones) are rapidly destroyed by upwelling (downwelling) favorable winds. None of these studies have considered the effects of lighter winds and reversals in the wind direction.

Simulations using constant wind directions are not altogether realistic. Figure 1.2 and Figure 1.3 show the wind pattern observed by Johannessen *et al.* (1987) and Morison *et al.* (1987), respectively, during MIZEX 84. The two observations show that there were periods when the wind shifted regularly, and also there were extended periods with light winds.

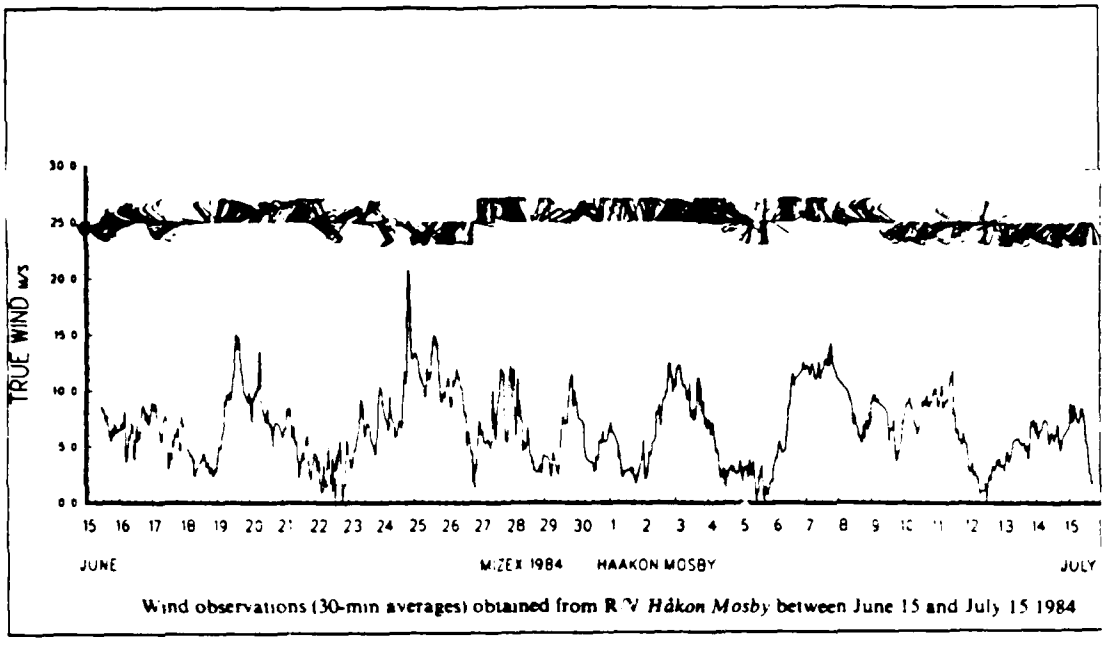

Figure 1.2 Time Series of Wind (from Johannessen *et al.* (1987)).

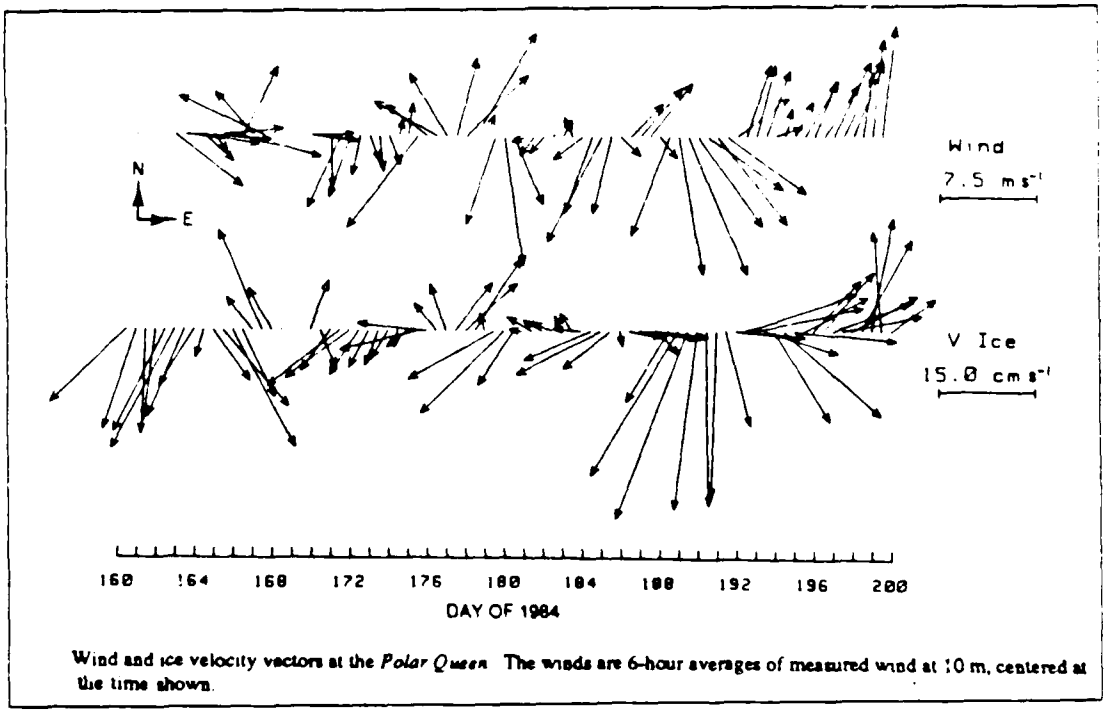

Figure 1.3 Time Series of Wind (from Morison *et al.* (1987)).

Johannessen *et al.* (1987) provide a schematic of the interaction of an open ocean eddy with the ice edge (Figure 1.4). This eddy (Johannessen *et al.* (1987), eddy (E13)) was observed for about eleven days. Figure 1.2 shows that for the first three days, steady winds along the ice were observed, followed by periods of lighter winds, varying in direction for periods of about one day. The last days of observation of this eddy were dominated by strong winds from the south, forcing the ice away from the eddy.

E. PURPOSE OF THIS STUDY

The objective of this study is to understand the interaction of mesoscale, and largely barotropic, eddies with a marginal ice zone through the use of a nonlinear two-layer regional ocean model with temporally varying winds and a coupled ice model.

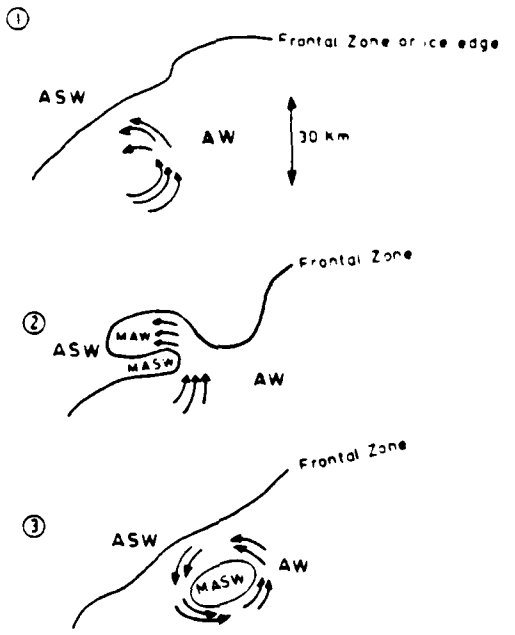

Schematic of the interaction of the open ocean eddy (E13) with the ice edge

Figure 1.4 Open Ocean Eddy Interacting with Ice Edge.

From Johannessen *et al.* (1987). Where AW is Atlantic Water, MAW is MIZ Atlantic Water, ASW is Arctic Slope Water, and MASW is MIZ Arctic Slope Water.

II. NUMERICAL TECHNIQUE AND MODEL PARAMETERS

A. OCEAN MODEL

1. Ocean Model Equations

Experiments are performed using a numerical model. The model is based on primitive equations, has two layers, and uses a semi-implicit numerical scheme. Motion in each layer is governed by a momentum equation:

$$\partial V_i/\partial t + (\nabla \cdot V_i + V_i \cdot \nabla)\, v_i + k \times f V_i = -h_i \nabla P_i + A_h \nabla^2 V_i + (\delta_{i1}/\rho_1)((1-A)\tau^{aw} + \tau^{iw}) \quad \text{(eqn 2.1)}$$

and a continuity equation:

$$\partial h_i/\partial t + \nabla \cdot V_i = 0 \quad \text{(eqn 2.2)}$$

for layer ($i = 1$ upper and $i = 2$ lower), thickness h_i, transports V_i, and velocities v_i. The fluid is hydrostatic, Boussinesq, and the fluid density (ρ_i) in each immiscible layer is fixed. Subgrid scale turbulent eddy dissipation processes are represented by a horizontal Laplacian operator on transport. As this only approximates a complex subgrid scale dissipation process, its coefficient, A_h, has been chosen small (10 m^2/s). The fluid is thus relatively inviscid. The notation used in all equations is defined in the Appendix. The above scheme has been used in numerous mid-latitude ocean mesoscale circulation studies (Hurlburt and Thompson (1980, 1982); Smith and O'Brien (1983)) where more thorough presentations show how energy and enstrophy are conserved in the absence of dissipation. Smith and Reid (1982) compared test cases to linear analytic solutions to verify the Rossby dispersion characteristics of the model.

2. Boundary and Initial Conditions

A rectangular (55 x 40 km) finite difference gridded domain is used. There are 55 grid points in the x-direction and 44 grid points in the y-direction. The domain is rotated counter-clockwise approximately 30 degrees relative to a reference latitude of 80°N so that the x-axis is aligned with the East Greenland Current, approximately parallel to the east coast of Greenland. The initial ocean state consists of a Gaussian height field in each layer, which is centered in the basin:

$$h_i = A_0 e^{(-(x^2+y^2)/2L^2))} \qquad \text{(eqn 2.3)}$$

L is the e-folding width scale for the eddy (= 5 km). The depth of thermocline in the East Greenland Current ranges from 25 to 100 m. All experiments for this study are initialized with the upper layer mean thickness of 50 m and the lower layer mean thickness of 4000 m. The resulting first internal Rossby radius of deformation (R_d) is equal to 5 km, consistent with the observations of Johannessen *et al.* (1983). Nondimensional eddy size, $\gamma = L/R_d$, is equal to 1. The amplitude (A_0) of the Gaussian distribution was chosen so that a maximum velocity would be on the order of 10 cm/s in each layer. Thus, the Rossby number (v_{max}/fL) for such a flow is 0.15; therefore, the nonlinear terms are expected to be important parameters in the momentum equations. The ocean velocity field is thus initially in gradient balance and constant with depth ($u_1 = u_2$). The north and south boundaries of the model domain are no-slip walls, where both tangential flow and normal flow are set equal to zero. Open radiation is allowed at the east and west boundaries of the model domain to allow wind-driven inflow and outflow. Simulations were integrated for short periods, typically 4 days. The sense of ocean eddy rotation (cyclonic vs. anticyclonic), wind direction, wind speed, and the duration of wind shifts were varied. Although the eddies are initialized with barotropic structure, baroclinic structure associated with wind-driven layer interface motion is free to evolve.

B. ICE MODEL

1. Ice Model Equations

Motion in the ice is governed by momentum equations:

$$\partial u/\partial t + u\partial u/\partial x + v\partial u/\partial y = fv - (A/m)(\tau_x^{ai} - \tau_x^{iw}) - g^*\partial(h_1 + h_2)/\partial x \qquad \text{(eqn 2.4)}$$

$$\partial v/\partial t + u\partial v/\partial x + v\partial v/\partial y = -fu - (A/m)(\tau_y^{ai} - \tau_y^{iw}) - g^*\partial(h_1 + h_2)/\partial y \qquad \text{(eqn 2.5)}$$

and by continuity equations:

$$\partial A/\partial t + \partial(Au)/\partial x + \partial(Av)/\partial y = A_a \nabla^2 A \qquad \text{(eqn 2.6)}$$

$$\partial m/\partial t + \partial(mu)/\partial x + \partial(mv)/\partial y = A_m \nabla^2 m \qquad \text{(eqn 2.7)}$$

for ice concentration (A) and ice mass (m). As in previous ice model studies, a Laplacian damping term has been included in the continuity equations for A and m. The ice equations contain a pressure force associated with sea surface slope. Most mesoscale modeling studies of the MIZ have neglected this term; Smith *et al.* (1987) show that this term is important in the absence of wind forcing. No internal ice stress was used, which is suitable for concentrations less than 85%. Thermodynamic effects are not considered in this study. The ice is coupled to the ocean through an ice-water interfacial stress, τ^{iw}, for ice (u) and ocean (u_w) velocity vectors:

$$\tau^{iw} = \rho_i c_{iw}(u-u_w)|u-u_w| \qquad \text{(eqn 2.8)}$$

and similarly the ice is coupled to the air through the air-ice interfacial stress, τ^{ai}, for air (u_a) and ice (u_{ice}) velocity vectors:

$$\tau^{ai} = \rho_a c_{ai}(u_a-u_{ice})|u_a-u_{ice}| \qquad \text{(eqn 2.9)}$$

All constant values (ρ_i, ρ_a, c_{iw}, c_{ai}) are chosen following Häkkinen (1986a) and are given in the appendix.

2. **Ice Thickness and Concentration**

The ice thickness distribution, D, is initially specified to be 2 meters thick, but is then allowed to vary according to

$$D = m/(\rho_i A) \qquad \text{(eqn 2.10)}$$

Ice concentration is initially a concentrated band in the middle of the domain. The ice band is a linear function of the y-coordinate, varying from 0.05 at the edge of the band nearest the open ocean to 0.75 at the edge of the ice band nearest the pack ice. The ice is initially at rest. The difference in value between adjacent contour lines of ice concentration found in the model output graphics is 0.05.

C. PRELIMINARY CONSIDERATIONS AND EXPECTED MODEL RESPONSE

Previous studies of isolated eddies have examined in detail the propagation and decay of isolated eddies in quiescent β-plane backgrounds (McWilliams and Flierl, 1979; Mied and Lindemann, 1979). At mid-latitudes, isolated eddies have significant propagation tendencies associated with the planetary vorticity gradient (β) and can decay through Rossby wave radiation and frictional processes. These studies showed that westward propagation speed is limited by the Rossby long wave speed:

$$c_{max} = -\beta R_d^2 \qquad \text{(eqn 2.11)}$$

The value of c_{max} at low latitudes is approximately 4 km/day; however, at 80°N, c_{max} is on the order of .01 km/day. The decay time associated with Rossby wave radiation (Smith and Reid, 1982) is substantially longer at high latitudes. Simulations reported here focus on the short time interaction (less than 1 week) of isolated eddies and ice. It is anticipated that eddy evolution and decay for these short time cases are related wind or to ice processes and not to the aforementioned processes, which occur on longer time scales.

The previous wind forced marginal ice zone ocean models give an indication of the expected Ekman response in the ocean and ice edge. Häkkinen (1986a, b) shows that 10 m/s along-ice-edge winds give an upwelled or downwelled interface amplitude of ~10 m and an ice edge jet velocity of 9 cm s after a 10-15 day spin-up period. Additionally, ice banding simulations require at least one wind reversal to occur. As simulations here are integrated for shorter periods with weaker winds, weak ice edge jet velocities and no ice banding are expected.

III. EXPERIMENTS

A. WIND FORCING DIRECTIONS

An understanding of the effect of wind direction on ice motion is the goal of the following experiments. Variable in the experiments are the wind magnitude, direction, and duration for a given direction. Values for wind direction are measured counterclockwise in degrees from the positive x-axis of the model domain. Since the model domain is rotated 30° counterclockwise, a model input wind direction of 025° means that on the globe, the wind would be generally from the southwest. This correlates to a downwelling favorable wind condition when viewed relative to the initial concentrated ice band. Table 1 lists the wind directions used in simulations.

TABLE 1
WIND DIRECTIONS USED IN SIMULATIONS

RELATIVE WIND	MODEL INPUT WIND	TRUE WIND
Upwelling Favorable	205°	235°
Downwelling Favorable	025°	055°
On-ice	115°	145°
Off-ice	295°	325°

A model input wind direction of 205° would be a true wind generally from the northeast; this correlates to an upwelling favorable wind. Winds perpendicular to the downwelling or upwelling wind directions are considered to be generally on-ice and off-ice winds. Along-ice-edge wind forcing (0° and 180°) induces a cross-ice-edge Ekman drift in the ice. The 025° and 205° angles chosen by Smith *et al.* (1987) are intended to minimize (but not eliminate) the cross-ice-edge motion, thereby maintaining the concentrated ice band near mid-domain and thus reducing boundary effects. The most

important aspect of these experiments is not the true direction of the wind, but the relative direction of the wind in relation to the concentrated ice band.

B. PRELIMINARY EXPERIMENTS

Before proceeding to the more realistic wind-driven simulations, the response of the ice edge to ocean eddies, without wind forcing, is considered first.

1. Simulations with No Wind

a. Cyclonic Eddy Initialization

Figure 3.1 shows the evolution of the concentrated ice band under the influence of a cyclonic ocean eddy without wind forcing. By day one, the eddy is affecting the ice band in such a way that the ice band contains a sinuous pattern that by day two is more pronounced. By day three the ice clearly exhibits a circular, cyclonically turning eddy, which is completely distinct from the original ice band by day four.

b. Anticyclonic eddy initialization

As would be intuitively expected, the anticyclonic case (Figure 3.2) with no wind forcing exhibits nearly the same result as above, except that the sense of rotation is opposite from the cyclonic case.

The results indicate that the ice velocity evolves rapidly to the ocean velocity and is simply advected radially. These results are consistent with Smith *et al.* (1987), where a broader ice concentration band was considered. Smith *et al.* (1987) show that the ice momentum equation in no wind simulations equilibrates to a gradient balance. For the cyclone case, a radially inward pressure force in the ice associated with the ocean surface slope is balanced by the radially outward Coriolis and centrifugal forces. Likewise, for an anticyclone case, the radially outward pressure gradient and centrifugal forces are balanced by the inward Coriolis force. The ice momentum balance was shown to equilibrate rapidly in less than one day.

C. BASE CASE

Numerous experiments were conducted using the model previously discussed. To assess the model output variations resulting from parameter changes, one simulation is chosen to be a base case. This simulation was selected as the reference case because of its resemblance to the observations of Johannessen *et al.* (1987). A summary of the model parameters chosen for the base case is listed in Table 2.

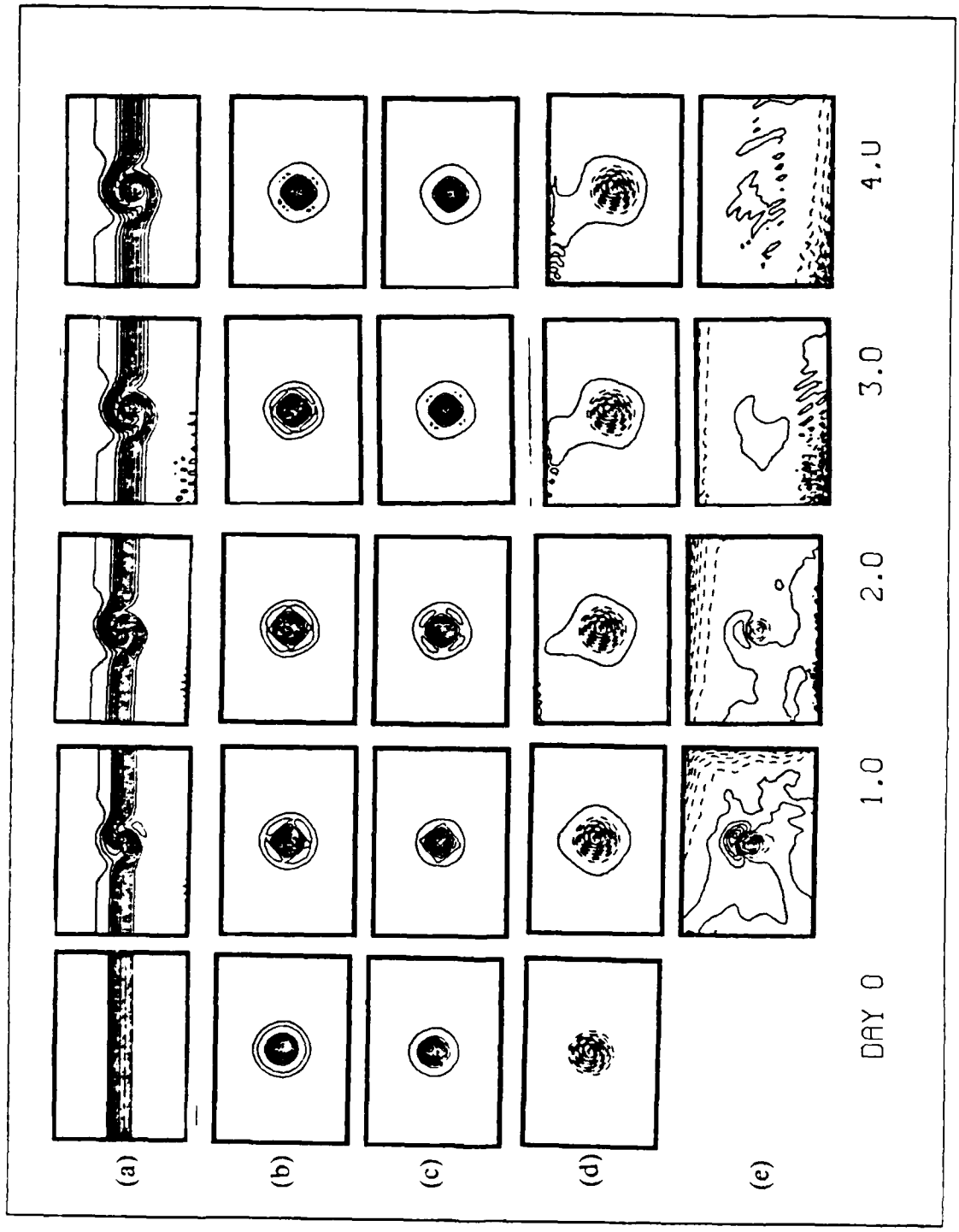

Figure 3.1 Preliminary Experiment (Cyclone).

Evolution of (a) ice concentration, (b) ocean upper layer potential vorticity, (c) ocean lower layer potential vorticity, (d) ocean surface height anomaly, and (e) ocean interface height anomaly. Contour interval for ice concentration is 0.05.

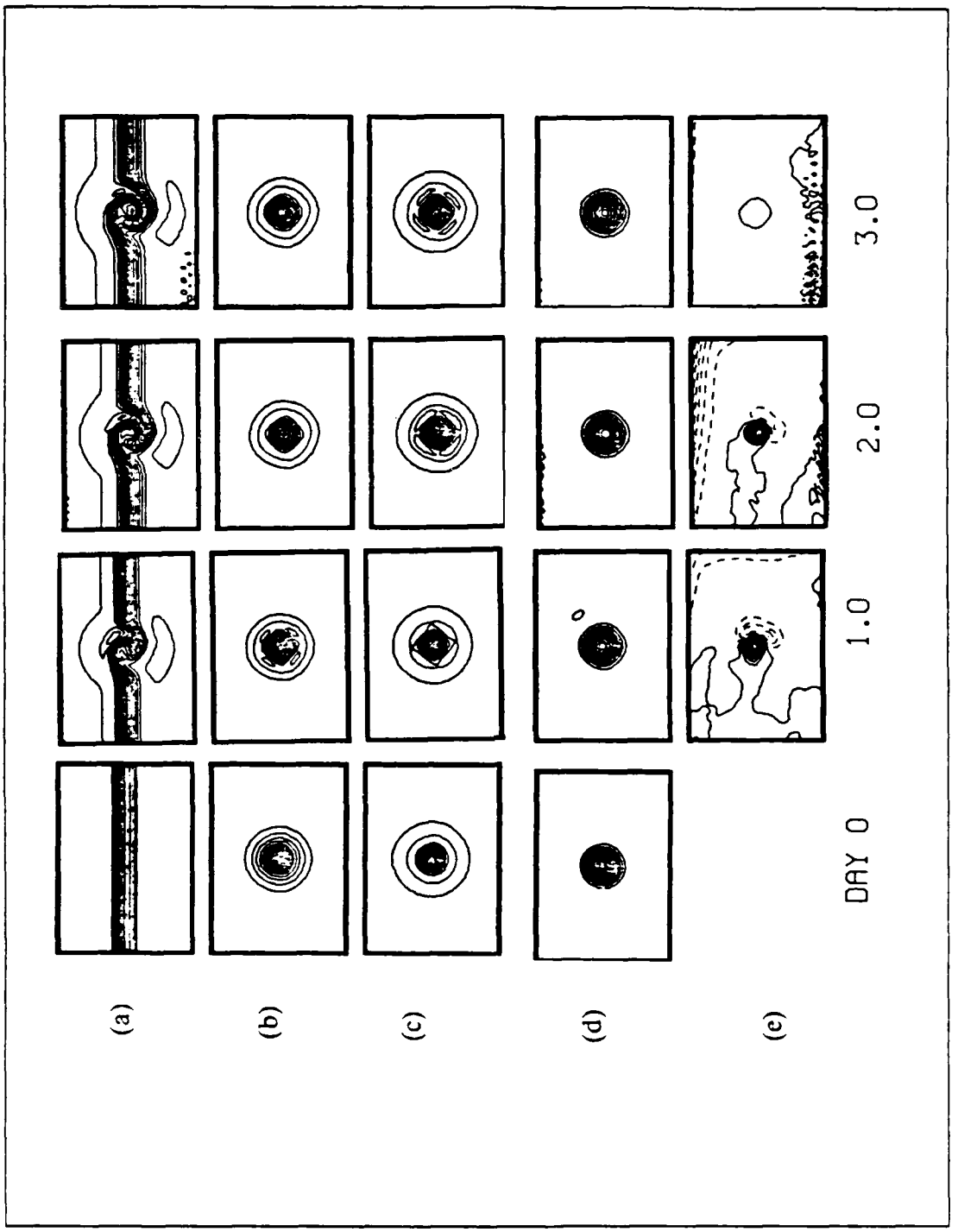

Figure 3.2 Preliminary Experiment (Anticyclone).

Evolution of (a) ice concentration, (b) ocean upper layer potential vorticity, (c) ocean lower layer potential vorticity, (d) ocean surface height anomaly, and (e) ocean interface height anomaly. Contour interval for ice concentration is 0.05.

TABLE 2
BASE CASE MODEL PARAMETERS

PARAMETER	SYMBOL	MODEL INPUT
Initial Upper Layer Thickness	H_1	50 m
Initial Lower Layer Thickness	H_2	4000 m
Initial Ice Thickness	D	2 m
Initial Ice Band Concentration	A	.05 to .75
Density of Ice	ρ_i	910 kg m^3
Grid Spatial Resolution	Δx	1000 m
Time Increment	Δt	600 s
Bottom Topography		Flat
Eddy Radius		5 km
Eddy Rotation		Cyclonic
Wind Speed		3 m s
Wind Direction		205°

1. **Experiment No. 1 (Base Case: Cyclone, Light Upwelling Winds)**

Using the input parameters listed in Table 2, an entire range of experiments can be discussed and compared to this reference case. Light winds (3 m s) were chosen because they are often observed, but until now have not been included in model simulations.

With constant light upwelling favorable winds (3 m s), the concentrated ice band responds to the cyclonic motion of the ocean eddy for the first day (see Figure 3.3). However, by day two, the effect of the wind causes a strong projection to the south of the ice band. This projection of more concentrated ice becomes an enclosed cyclonic feature by day three. By day four the cyclonic feature has nearly broken away from the original concentrated ice band. As a result of the growth of the projection first noted at day two, there is a pocket of more concentrated ice that is cut off from ice of equal concentration that has formed to the south. Also evident in the figure is a

significant northward Ekman drift of the ice edge; the resulting signature of the ocean eddy in the ice is dependent upon cross-ice-edge motion. Figure 3.3 also shows that 3 m s winds produce no noticeable effect on the upper ocean cyclone. Figure 3.3 also shows that insignificant upwelling occurs for this wind magnitude. The interface anomaly indicates downwelling at the top boundary of the model domain and upwelling at the bottom boundary of the model domain as expected from considerations of Ekman-induced motion at a boundary. Figure 3.4 shows the ice pattern concentration at day four and day five.

Figure 3.5 shows how the velocity of the ice is affected by the wind and the ocean eddy for the base case. The ice toward the upper (northern) boundary, over the ocean eddy, is moving faster than the ice located toward the bottom (southern) boundary, over the ocean eddy. The northern ice moves faster because the ocean eddy and the wind are working together; in the southern part of the model domain, the ocean-eddy-driven component and the wind-driven component of ice motion are opposed.

The ice momentum balance for 10 m s wind driven cases is shown in Smith *et al.* (1987). The gradient ice momentum balance seen above in no wind cases becomes a secondary balance. The dominant force balance in the ice becomes that between τ^{ai}, the air-ice stress in the direction of the wind, and τ^{iw}, the ice-water drag.

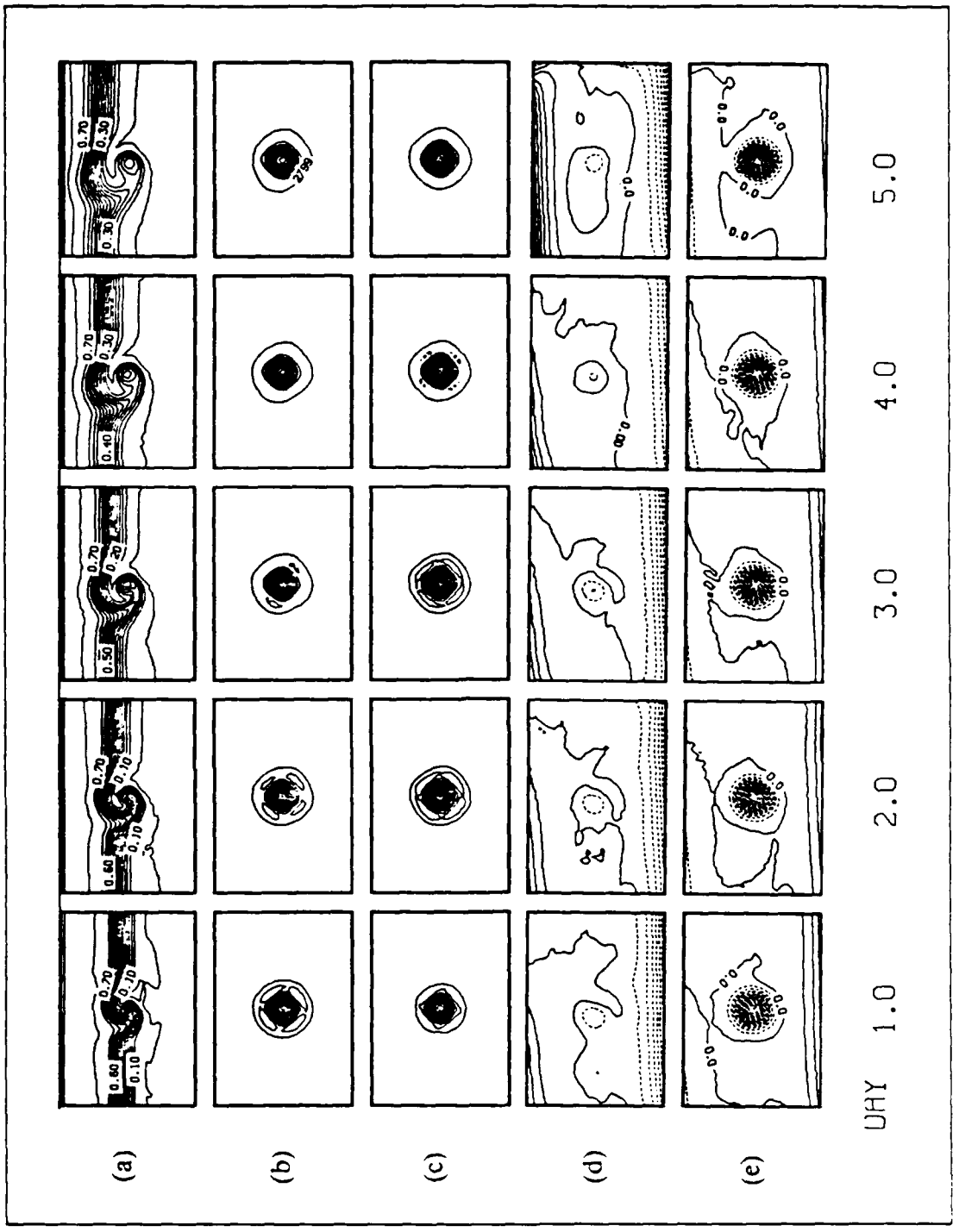

Figure 3.3 Experiment No. 1 (Base Case).

Evolution of (a) ice concentration, (b) ocean upper layer potential vorticity, (c) ocean lower layer potential vorticity, (d) ocean surface height anomaly, and (e) ocean interface height anomaly. Contour interval for ice concentration is 0.05.

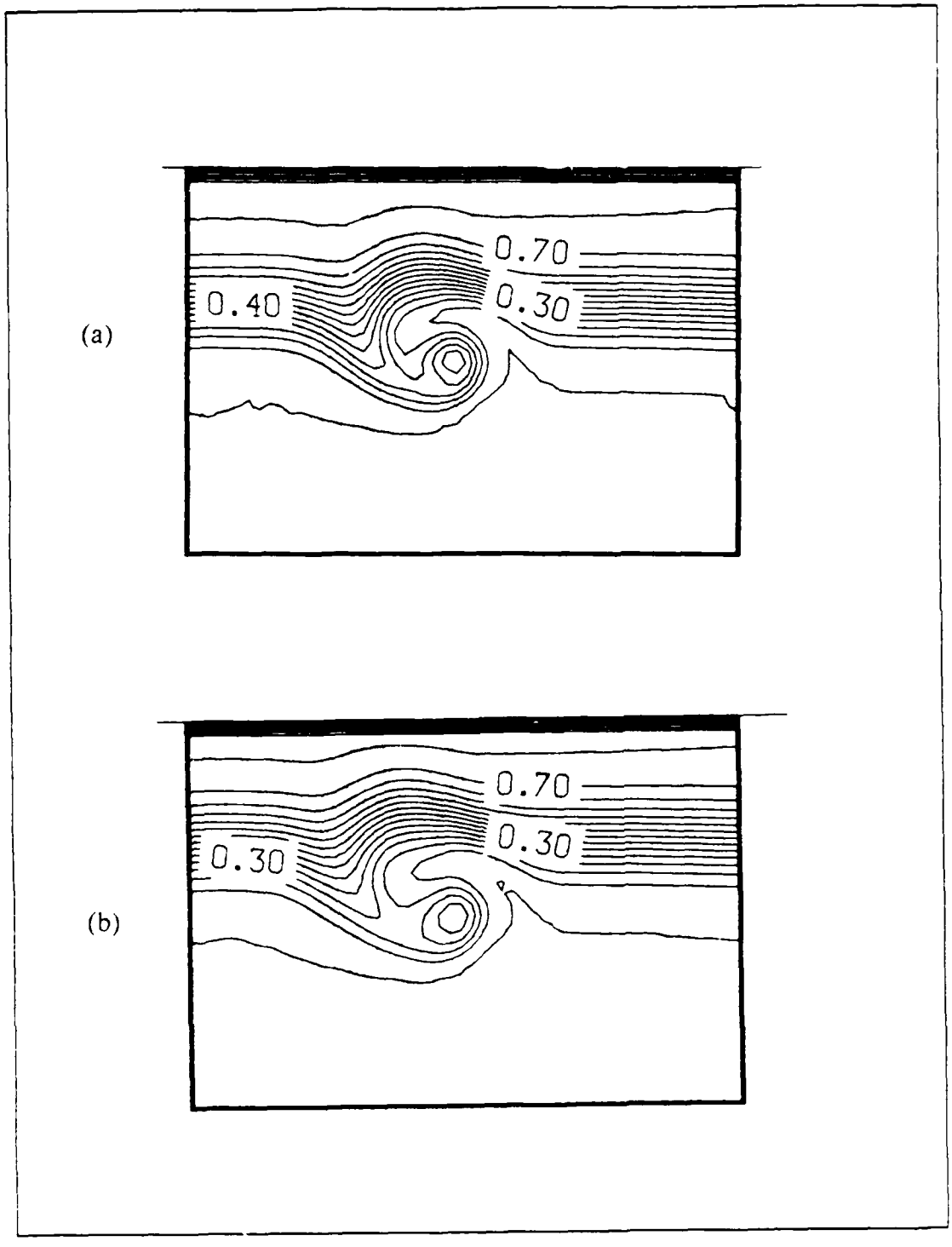

Figure 3.4 Experiment No. 1 (Base Case).

Ice concentration at (a) day 4 and (b) day 5. Contour interval for ice concentration is 0.05.

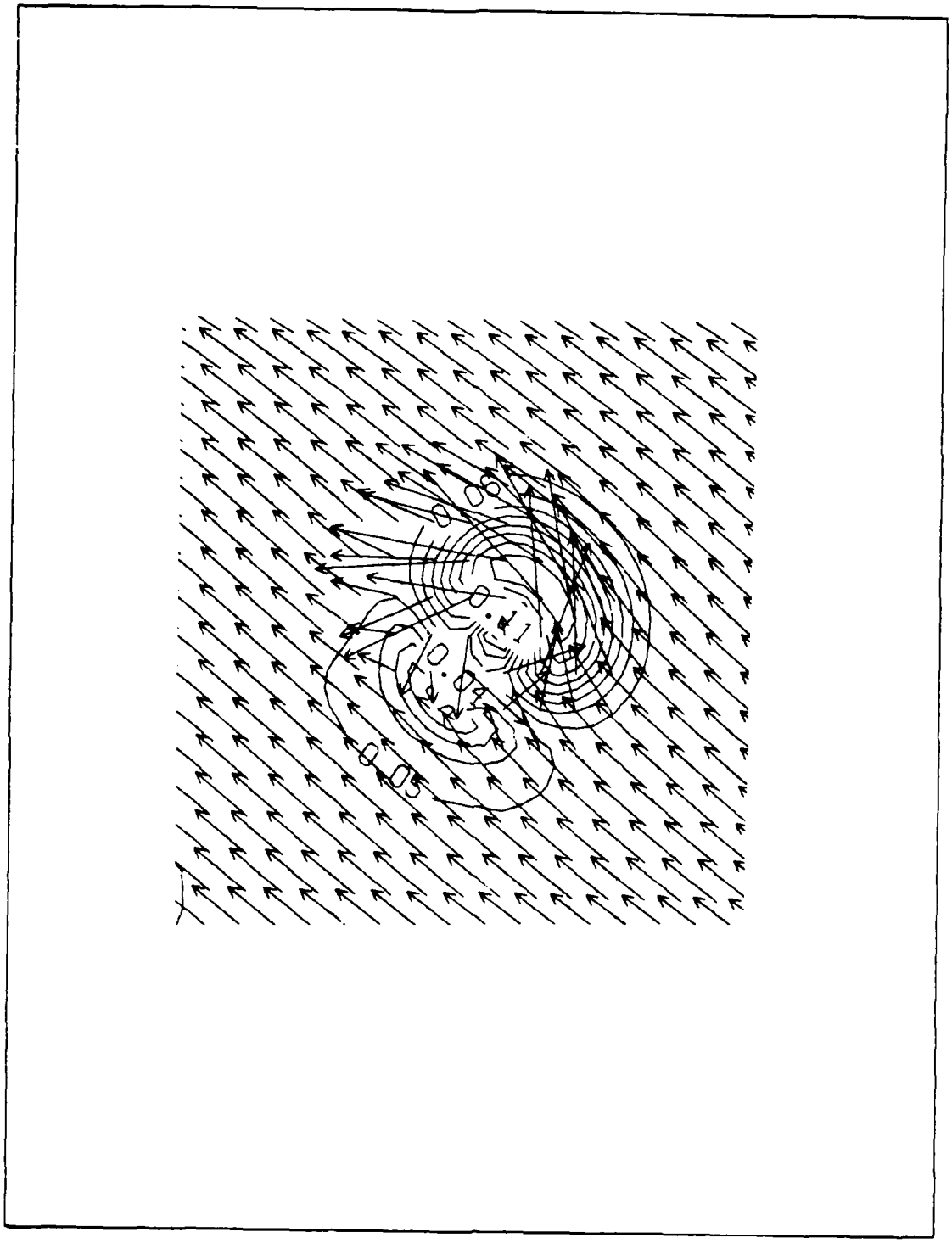

Figure 3.5 Plots of Ice Velocity (Base Case).

Ice velocity vectors at day 3. Arrows represent ice velocity. Contours highlight areas of high or low velocities.

D. VARIATION FROM THE BASE CASE

Table 3 lists the model parameters that are varied in the experiments, beginning with Experiment No. 1 (base case). Since the observations of Johannessen *et al.* (1987) indicate that most of the mesoscale eddies observed in the East Greenland Current MIZ are cyclonic, most of the experiments are for cyclonic eddies.

TABLE 3
MODEL PARAMETERS VARIED IN EXPERIMENTS

EXP #	OCEAN EDDY	WIND DIRECTION	WIND SPEED	WIND SHIFT
1	cyclonic	205°	3 m s	no
2	anticyclonic	205°	3 m s	no
3a	cyclonic	025°	3 m s	no
3b	cyclonic	025°	5 m s	no
4	anticyclonic	025°	3 m s	no
5a	cyclonic	205° 25°	10 m s	24 hr
5b	cyclonic	205° 25°	10 m s	36 hr
6a	cyclonic	205° 115°	3 m s	24 hr
6b	cyclonic	205° 295°	3 m s	24 hr

1. Experiment No. 2 (Anticyclone, Light Upwelling Winds)

This experiment was conducted to observe the effect on the concentrated ice band of an anticyclonic ocean eddy in an environment similar to that of the base case. The anticyclonic eddy exhibits no development of a distinct cut-off feature (Figure 3.6) as in the cyclonic base case with 3 m s winds. The sinuous pattern in the concentrated ice band gives evidence of anticyclonic motion at day one, which becomes pronounced at day two, but by day three the anticyclonic signature is decreasing. By day four the ice pattern, which appears distinctly different from previous cases, is weakly anticyclonic but by no means representative of the anticyclonic eddy that is beneath the ice. Smith *et al.* (1987) found that 10 m s wind in this direction could destroy the upper ocean cyclone.

Figure 3.6 shows that there is no great change in the upper ocean vorticity pattern or upper layer pressure, indicating that 3 m s winds are of insufficient strength to alter the upper ocean eddy. However, this experiment shows that 3 m s winds have a significant effect on the ice. This case also shows the cross-ice-edge drift of the concentrated ice band to the north. Figure 3.7 shows how the velocity of the ice is affected by the wind and the ocean eddy for this case. In this case the wind and ocean are opposing effects, which results in the relatively flat ice pattern by day three.

2. **Experiments No. 3a, 3b (Cyclone, Downwelling Winds)**

a. Case for 3 m/s Winds

Experiment 3a (Figure 3.8) was designed to investigate the change in ice pattern for winds from a direction opposite from the base case. The initial conditions for this experiment are the same as Experiment No. 1 (base case), with the exception of the wind direction, which is changed 180° from the base case so that a downwelling favorable wind is used. With these opposite direction winds, no distinct cut-off feature develops, unlike the base case. At no point in time is there a concentration of ice over the eddy similar to that found in the base case. By day five there is little evidence from the ice pattern of a cyclonic ocean eddy under the ice, even though the potential vorticity of the ocean eddy remains nearly at the same value as that at day zero. Note also that the cross-ice-edge drift is now to the south, opposite from that for upwelling favorable wind conditions. The southward movement of the concentrated ice band creates a situation that is unfavorable for any distinct ice pattern to break away from the ice band.

The differences in the upwelling and downwelling cases can be understood from vorticity considerations. The air-ice stress τ^{ai} is weighted by ice concentration, A, in the ice momentum equations. Therefore, moving from high concentration toward low concentration, the air-ice coupling becomes weaker. Upwelling winds thus provide cyclonic vorticity to the ice and downwelling winds provide anticyclonic vorticity to the ice. The winds thus augment the ocean induced ice motion in the cyclone case and are opposed to the ocean induced ice motion in the anticyclone case.

b. Case for 5 m/s Winds

Case 3b (Figure 3.9) is the same as the above case with the wind increased to 5 m s from the previous 3 m s. This small increase shows how much quicker the response of the ice pattern is to slightly greater wind forcing. Other experiments, not shown here, show that as the wind speed continues to increase for the downwelling

favorable direction, the ice pattern responds sooner. This illustrates that the wind begins to dominate the ice momentum balance over the ocean forcing as winds increase from 3 m/s. Figure 3.9 shows that 5 m/s winds begin to induce a downwelled response at the ice edge near the end of 5 days. The upper ocean pressure field indicates a weakening of the ocean cyclone. Also evident is an increased cross-ice-edge motion to the south of the model domain.

3. **Experiment No. 4 (Anticyclone, Downwelling Winds)**

This experiment (Figure 3.10) was done to observe the effect of an anticyclone in the presence of downwelling favorable winds. Based on the results of Smith *et al.* (1987), the expections were that the anticyclonic signature in the ice would not be destroyed as quickly as in Experiment No. 2 where upwelling favorable winds were modeled. The anticyclonic signature is more pronounced because the vorticity input to the ice from the ocean and air are both anticyclonic; in Experiment No. 2 the vorticity input to the ice form the ocean and air are opposed.

For the first two days of this simulation, the anticyclonic signature in the ice develops much the same as in the cyclonic simulation (Experiment 3a), but with an opposite sense of rotation. The difference between this simulation and the base case is that instead of having a higher ice concentration over the ocean eddy center, a region of less concentrated ice becomes centered over the ocean eddy. Another difference is the shape of the lower ice edge of the concentrated ice band. In this case (Figure 3.11) the lower ice edge is smoother and less remarkable than found in the base case.

By the above arguments of vorticity input to the ice induced by the wind, this case should be the mirror image of the base case. A comparison of Figure 3.10 to Figure 3.3 shows this not to be the case. The explanation for his lack of symmetry lies in the Ekman induced cross-ice-edge component of motion. In the base case, the ice band drifted northward, away from the stationary ocean eddy. In this simulation the ice band has a southward drift, bringing higher ice concentration across the ocean eddy.

4. **Experiments No. 5a, 5b (Cyclone, 180° Reversal in Winds)**

For comparison with the results of Smith *et al.* (1987), where 10 m/s constant direction winds are considered, wind reversals are included next.

a. Case for 10 m/s Winds with 24 Hour Reversal

This experiment (Figure 3.12) shows the results of 10 m/s winds being instantaneously reversed from upwelling favorable winds to downwelling favorable

winds every 24 hours. This was repeated for a total of six days. Using this technique, the ice showed much the same response as the case with no wind; however, the ice over the eddy is somewhat more loosely packed. This experiment shows the vast difference in the ice pattern by including a wind shift in the model. By applying the results of Experiment No. 3b, a 10 m/s downwelling wind would quickly dominate the ice pattern initially induced by the ocean eddy. However, by daily reversals of the direction of the wind, the wind works in conjunction with the eddy to form a concentrated ice pattern over the ocean eddy. In terms of vorticity, the wind is alternately providing cyclonic (during upwelling) and anticyclonic (during downwelling) relative vorticity to the ice.

This experiment was also repeated using a number of other wind speeds. The results were similar; for each case with wind speeds less than 10 m/s, ice spirals radially over the eddy when the wind is shifted every 24 hours. This is in contrast to the results of Smith *et al.* (1987), where a 10 m/s wind was shown to straighten the ice edge, overcoming the effect of the ocean eddy. In Smith *et al.* (1987) it was also shown that constant direction upwelling (downwelling) winds destroyed an upper ocean cyclone (anticyclone). With wind reversals of 24 hours, this eddy destruction mechanism no longer is observed. This is consistent with a vorticity argument provided by Smith *et al.* (1987). As air-ice coupling is stronger than air-water coupling by virtue of the drag coefficients, the momentum input to the ocean by winds is larger under the ice than in the open ocean. Upwelling (downwelling) winds hence provide cyclonic (anticyclonic) vorticity to the upper ocean. In 24 hour wind reversals here, the wind alternately provides cyclonic and anticyclonic relative vorticity, thus allowing the ocean eddy to persist. Figure 3.13 shows the vorticity in the ice for a concentrated ice band with no eddy in the presence of upwelling and downwelling winds.

b. Case for 10 m/s Winds with 36 Hour Reversal

All other parameters are the same as the previous case, except that the wind shifts at 36 hour intervals. The difference in the ice pattern evolution is very striking. This case (Figure 3.14) does not develop a concentrated ice formation over the ocean eddy. The concentrated ice band shape is irregular throughout the simulation. The ice pattern gives no strong evidence of an ocean eddy, even though the ocean eddy persists during this period.

5. Experiments No. 6a, 6b (Daily 90° Shift in Light Winds)

a. Shift from Upwelling to On-Ice Winds with a Cyclonic Eddy

Here the wind was chosen as in the base case with a wind speed of 3 m s. In this experiment (Figure 3.15) the wind was shifted 90° back and forth every 24 hours, so that the wind would shift from upwelling favorable to on-ice after 24 hours, then shift back after the next 24 hours. The wind shift was continued for four days. The ice pattern develops a strong cyclonic cut-off feature at the eastern edge of the concentrated ice band that is much more pronounced than the cut-off feature to the bottom of the model domain found in any previous experiment. The wind from the southeast is an on-ice wind, which drives the concentrated ice band to the top of the model domain. The effect on the ice of upwelling winds with a cyclonic ocean eddy alone creates a near-break-away. The addition of on-ice winds greatly increases the concentration of the southward projection away from the concentrated ice band (Figure 3.16). The enhancement of cross-ice-edge motion by shifting the wind shows how sensitive the response of the ice is to the wind direction.

b. Shift from Upwelling to Off-Ice Winds with a Cyclonic Eddy

In this case the wind is shifted from upwelling favorable to off-ice winds every 24 hours. Figure 3.17 shows that the amount of ice over the ocean eddy in this case is less than in the on-ice case. This is due to the competing forces driven by the wind and the ocean eddy.

A comparison to the results of this simulation with the base case illustrates an important point. The breaking away of ice from the ice edge is dependent upon the ice edge retreating away from the eddy. In this simulation, no cross-ice-edge motion occurs and, hence, no break away of ice from the edge occurs. Thus, the process of ice trapping over eddies is sensitive to wind direction and the resulting cross ice edge shifts.

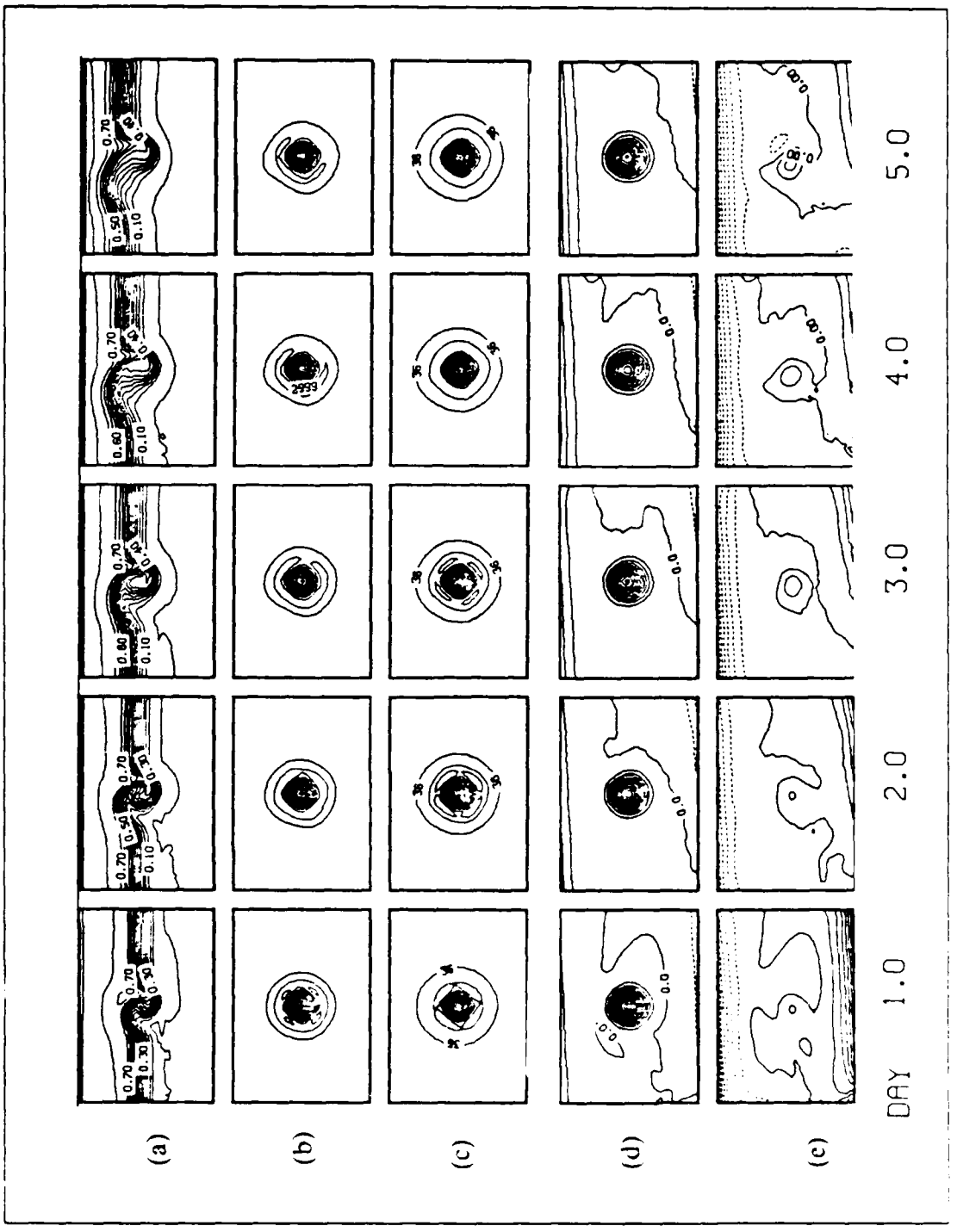

Figure 3.6 Experiment No. 2 (Anticyclone, Upwelling Winds).

Evolution of (a) ice concentration, (b) ocean upper layer potential vorticity, (c) ocean lower layer potential vorticity, (d) ocean surface height anomaly, and (e) ocean interface height anomaly. Contour interval for ice concentration is 0.05.

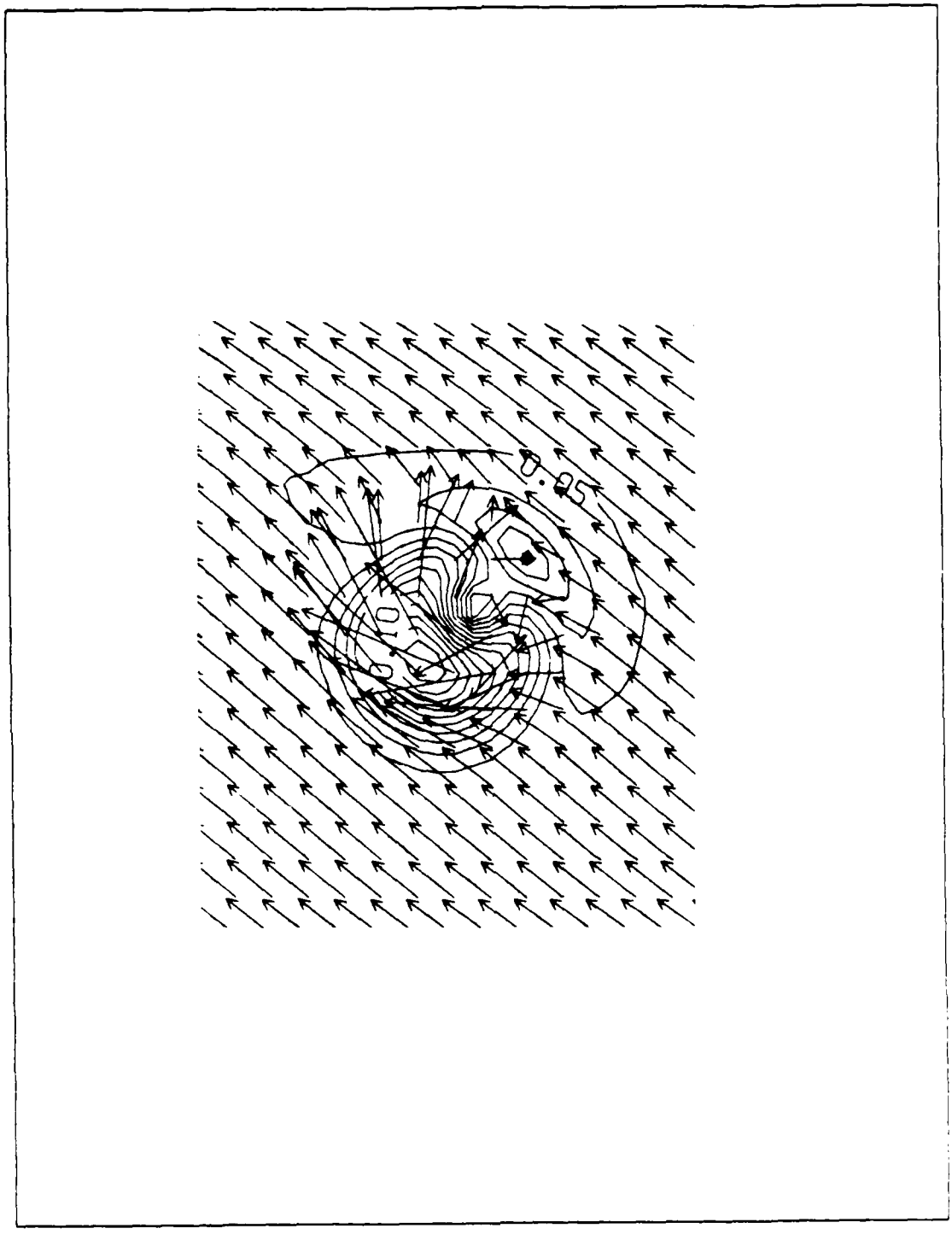

Figure 3.7 Experiment No. 2 (Anticyclone, Upwelling Winds).

Ice Velocity Vectors at day 3. Arrows represent ice velocity. Contours highlight areas of high or low velocities.

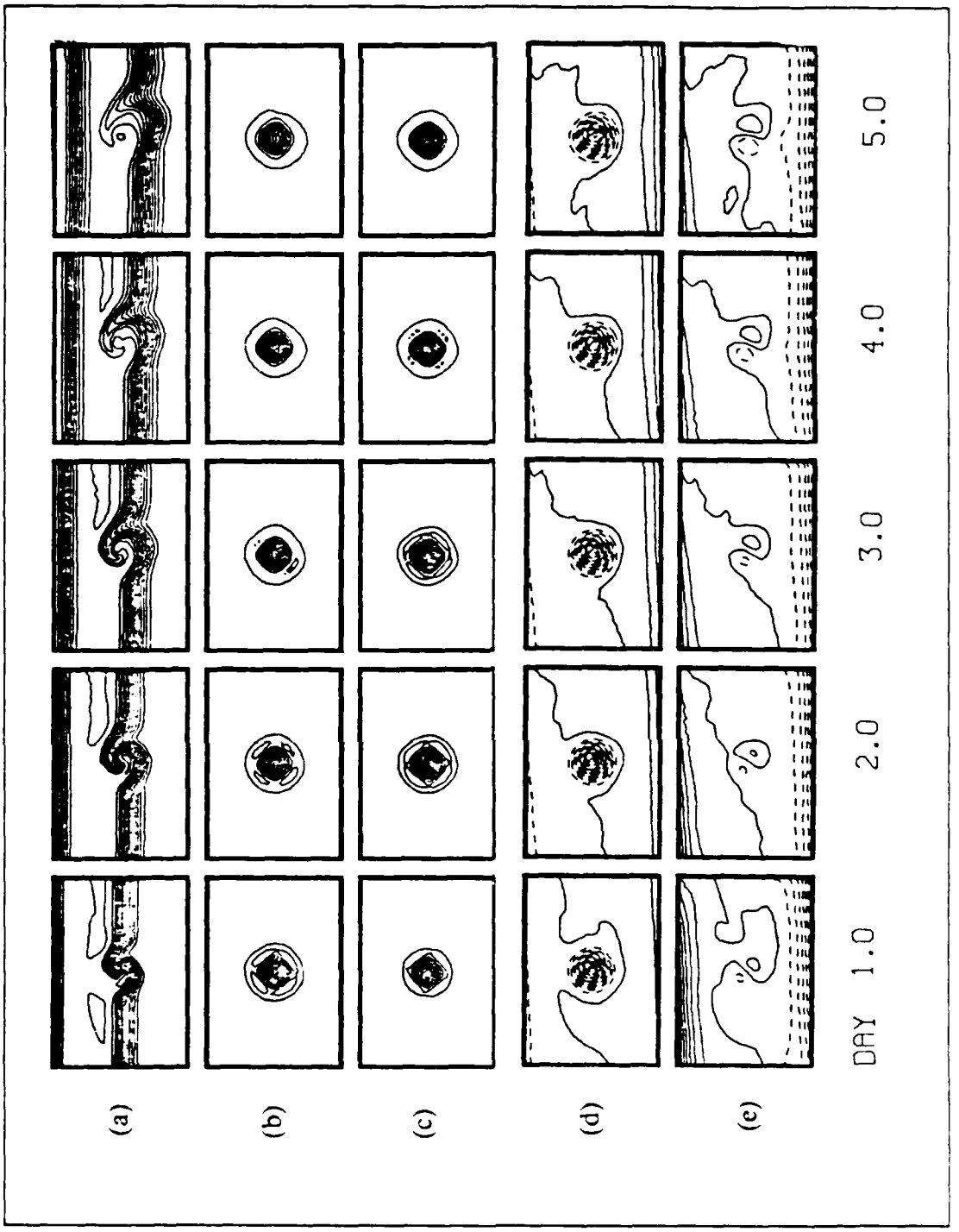

Figure 3.8 Experiment No. 3a (Cyclone, Light Downwelling Winds).

Evolution of (a) ice concentration, (b) ocean upper layer potential vorticity, (c) ocean lower layer potential vorticity, (d) ocean surface height anomaly, and (e) ocean interface height anomaly. Contour interval for ice concentration is 0.05.

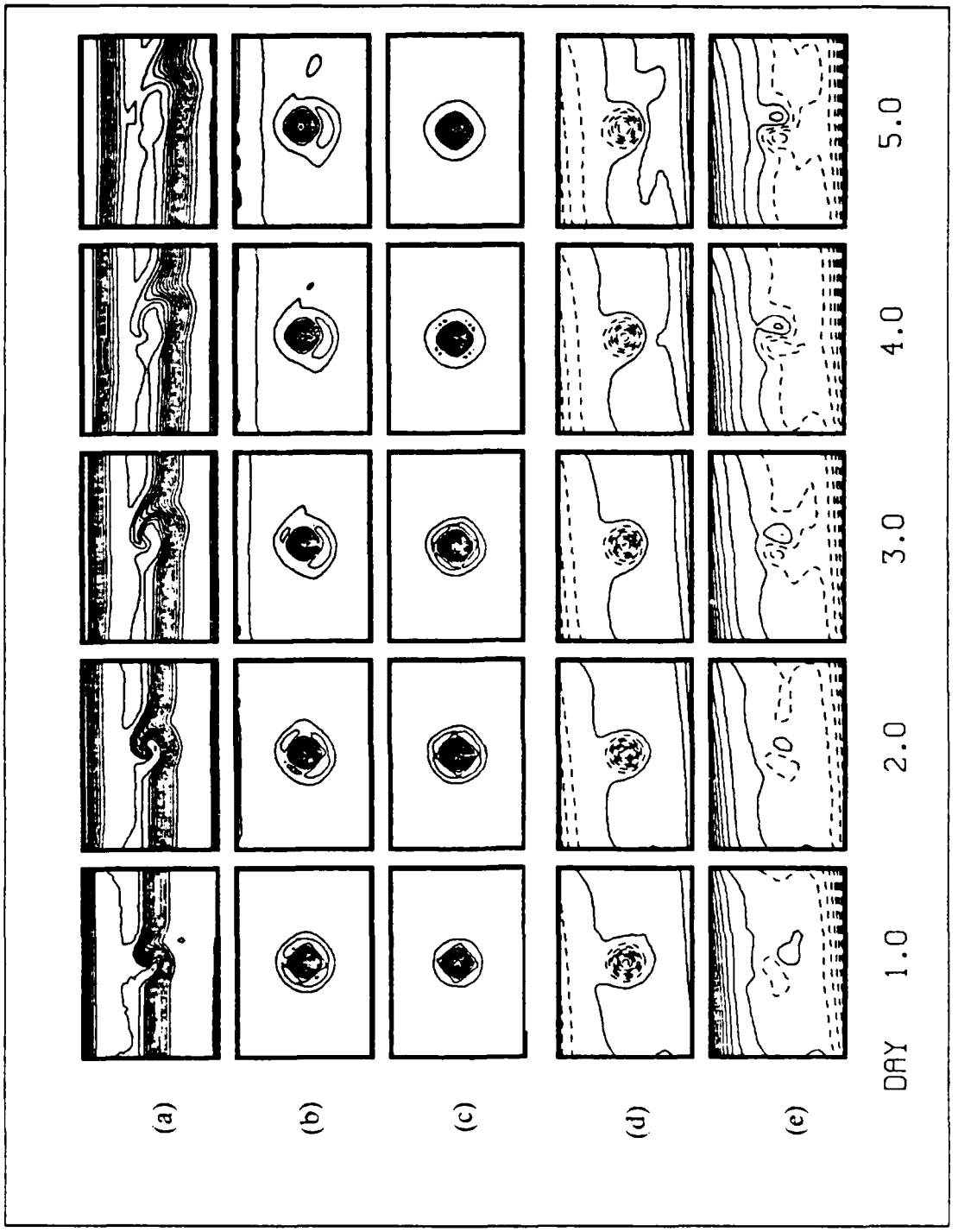

Figure 3.9 Experiment No. 3b (Cyclone, 5 m/s Downwelling Winds).

Evolution of (a) ice concentration, (b) ocean upper layer potential vorticity, (c) ocean lower layer potential vorticity, (d) ocean surface height anomaly, and (e) ocean interface height anomaly. Contour interval for ice concentration is 0.05.

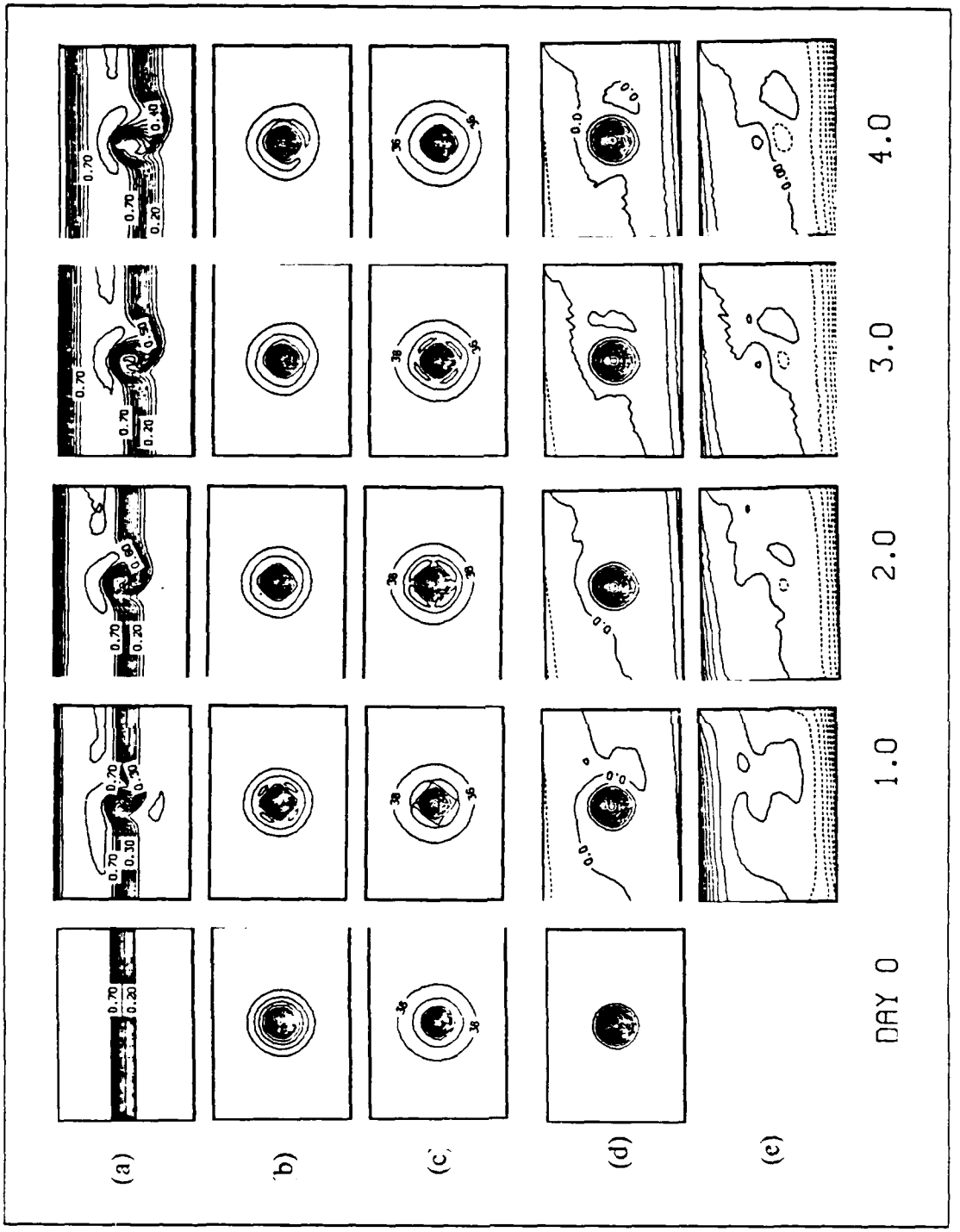

Figure 3.10 Experiment No. 4 (Anticyclone, Light Downwelling Winds).

Evolution of (a) ice concentration, (b) ocean upper layer potential vorticity, (c) ocean lower layer potential vorticity, (d) ocean surface height anomaly, and (e) ocean interface height anomaly. Contour interval for ice concentration is 0.05.

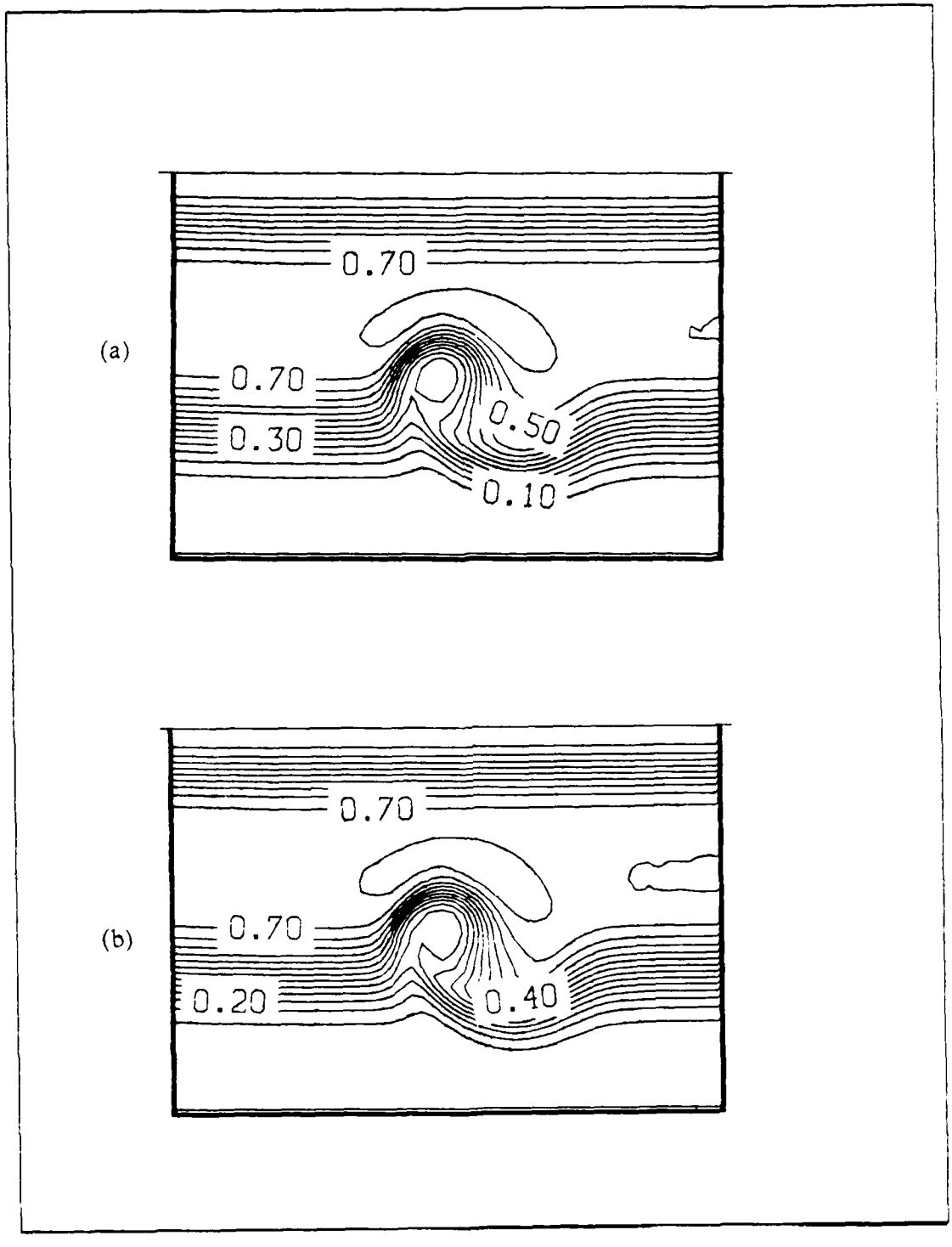

Figure 3.11 Experiment No. 4 (Anticyclone, Downwelling Winds).

Ice concentration at (a) day 4 and (b) day 4.5. Contour interval for ice concentration is 0.05.

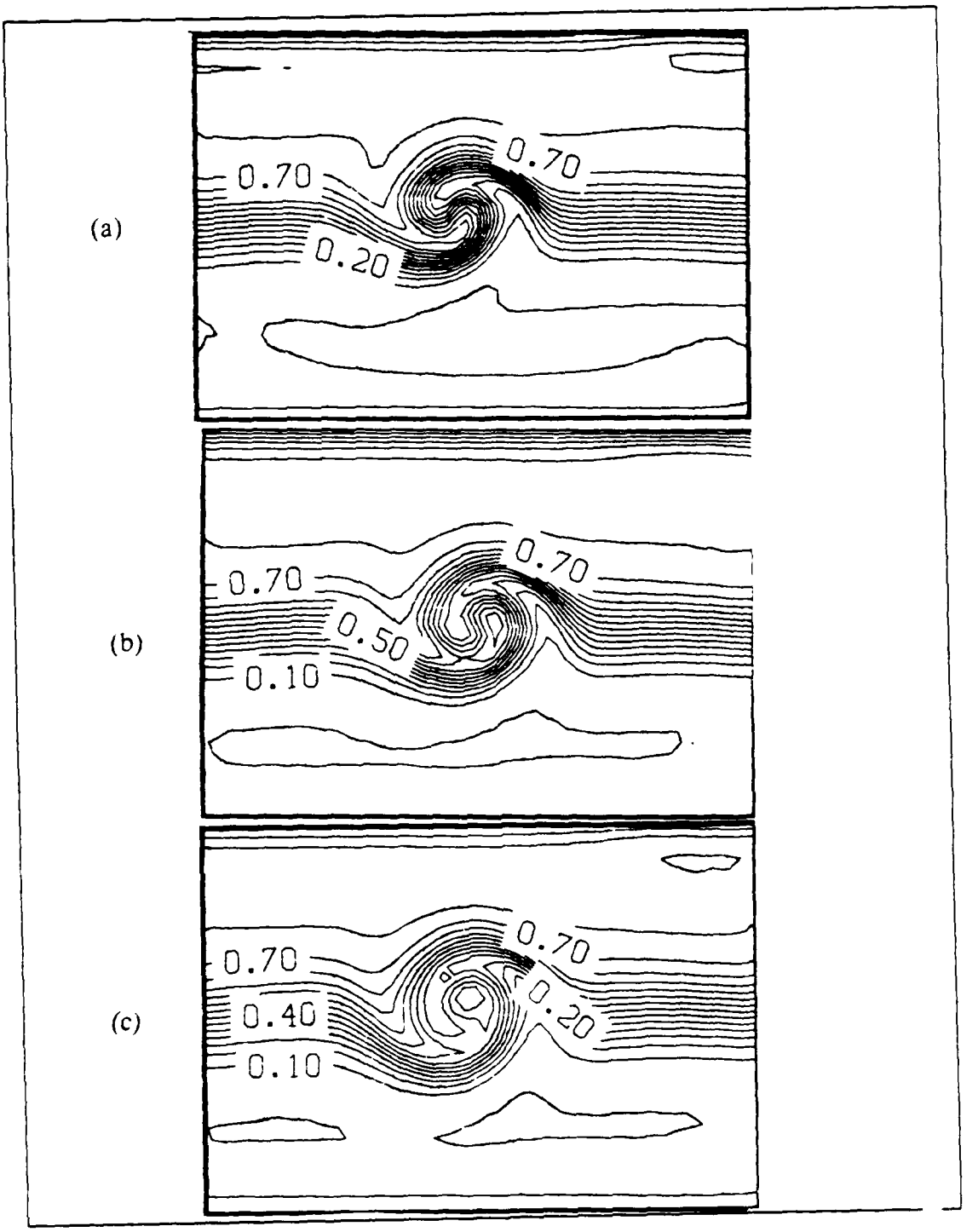

Figure 3.12 Experiment No. 5a (Cyclone, Daily 180° Reversal in 10 m/s Winds).

Ice concentration at (a) day 3 (b) day 4 and (c) day 5. Contour interval for ice concentration is 0.05.

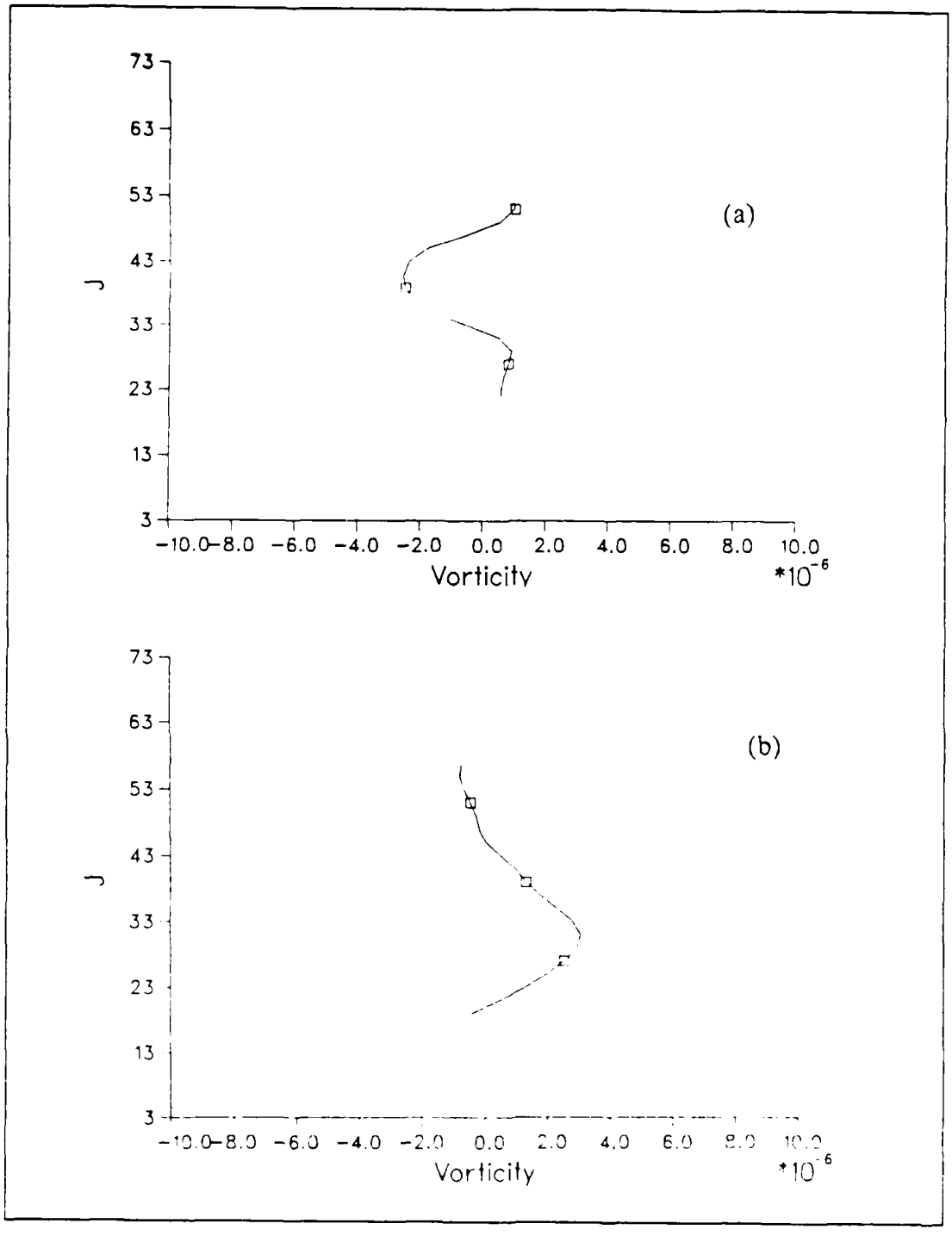

Figure 3.13 Vorticity Input to the Ice.

Vorticity across the ice band for (a) downwelling winds and (b) upwelling winds. Where J is the y-coordinate grid point.

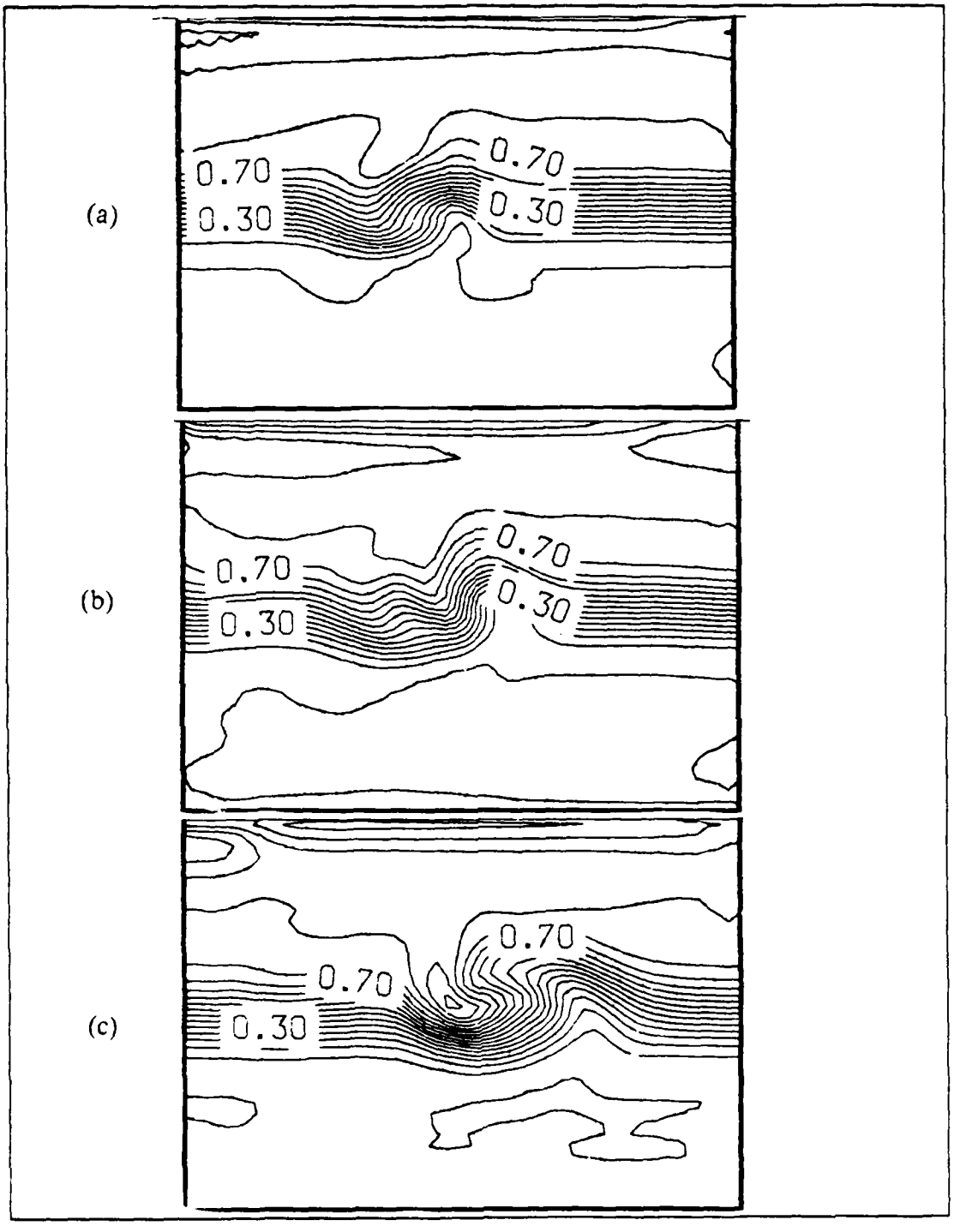

Figure 3.14 Experiment No. 5b (Cyclone, 36 hr 180° Reversal in 10 m/s Winds).

Ice concentration at (a) day 1 (b) day 2 and (c) day 3. Contour interval for ice concentration is 0.05.

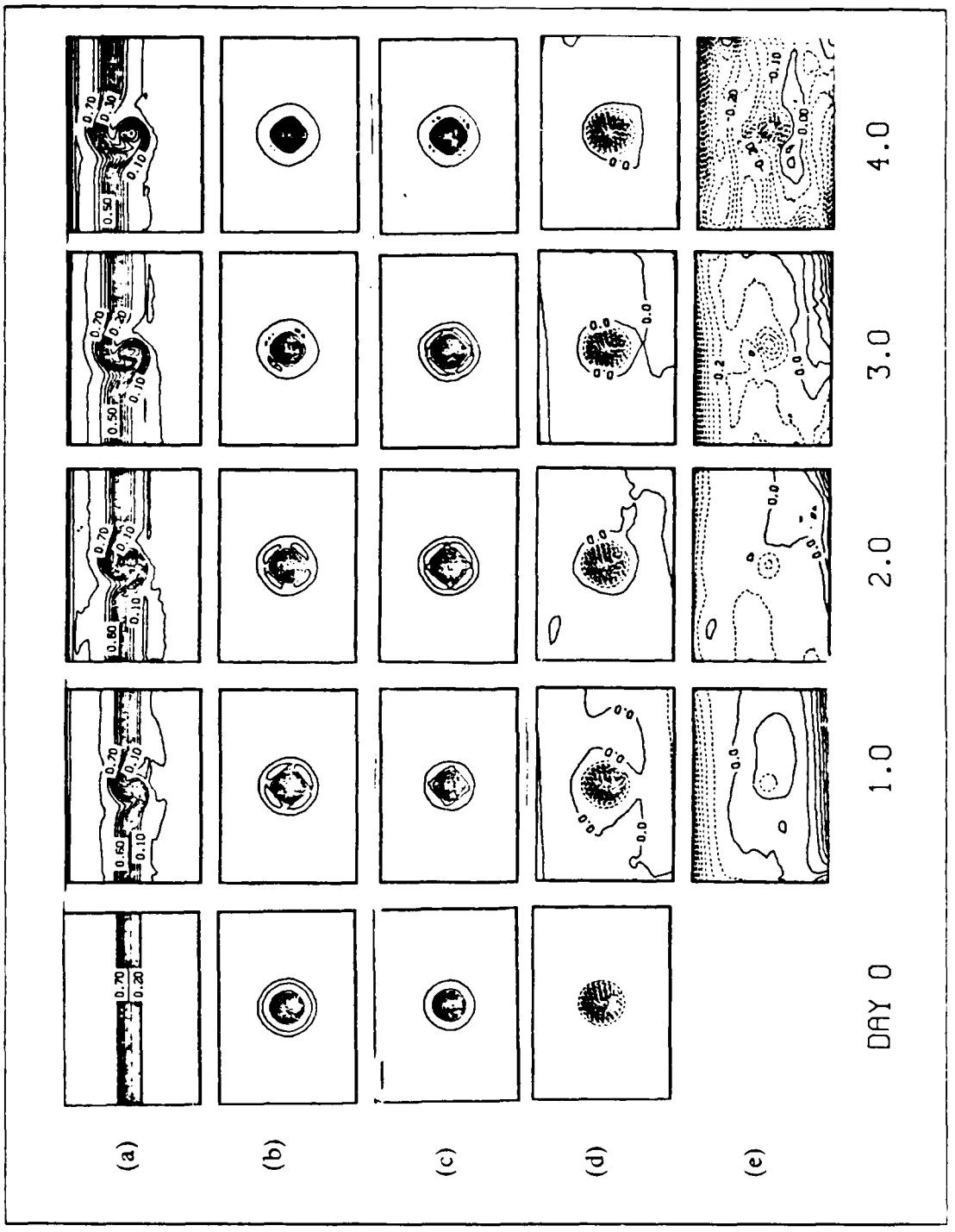

Figure 3.15 Experiment No. 6a (Cyclone, Daily 90° Shift to Light On-Ice Winds).

Evolution of (a) ice concentration, (b) ocean upper layer potential vorticity, (c) ocean lower layer potential vorticity, (d) ocean surface height anomaly, and (e) ocean interface height anomaly. Contour interval for ice concentration is 0.05.

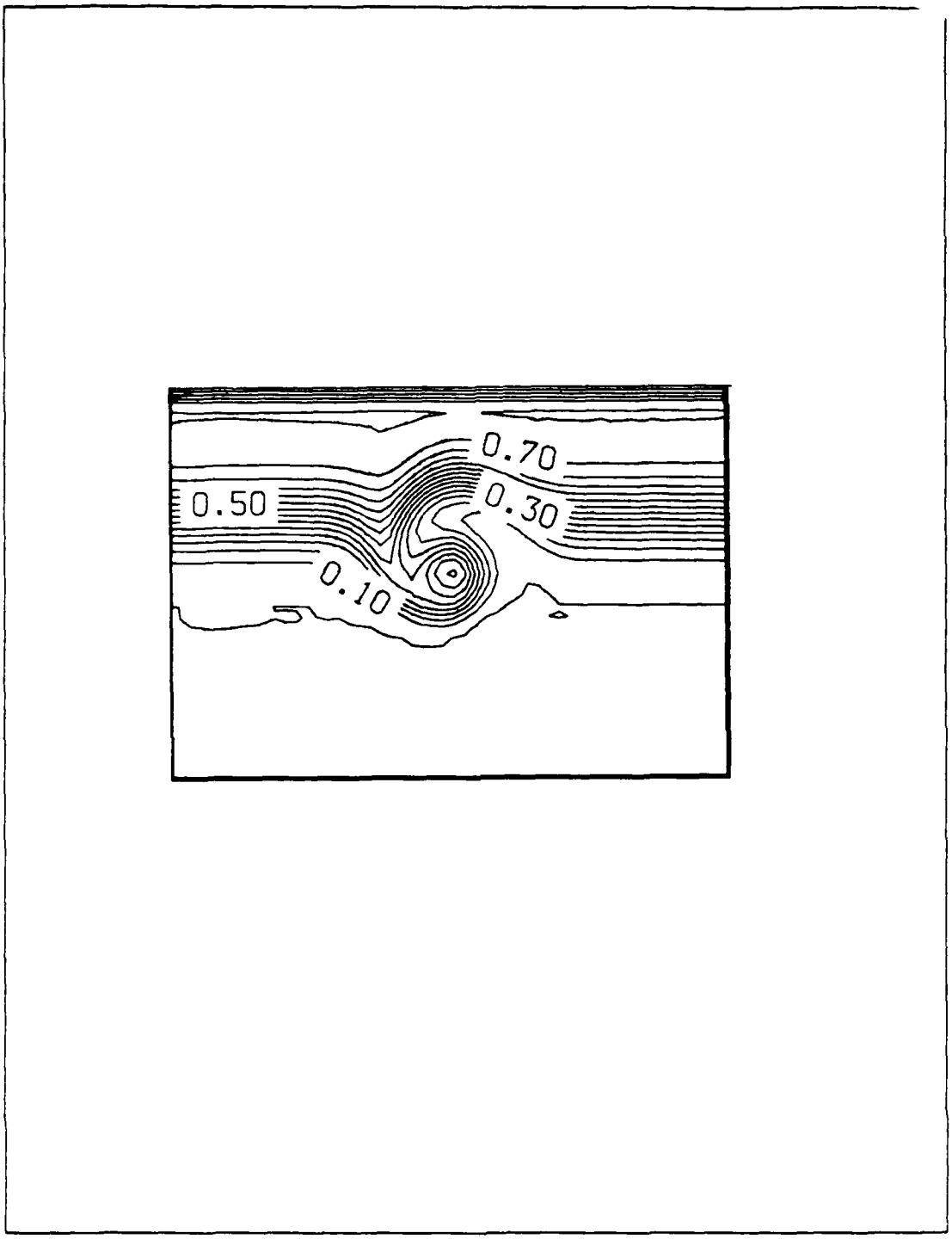

Figure 3.16 Experiment No. 6a (Cyclone, Daily 90° Shift to Light On-Ice Winds). Ice concentration at day 4. Contour interval for ice concentration is 0.05.

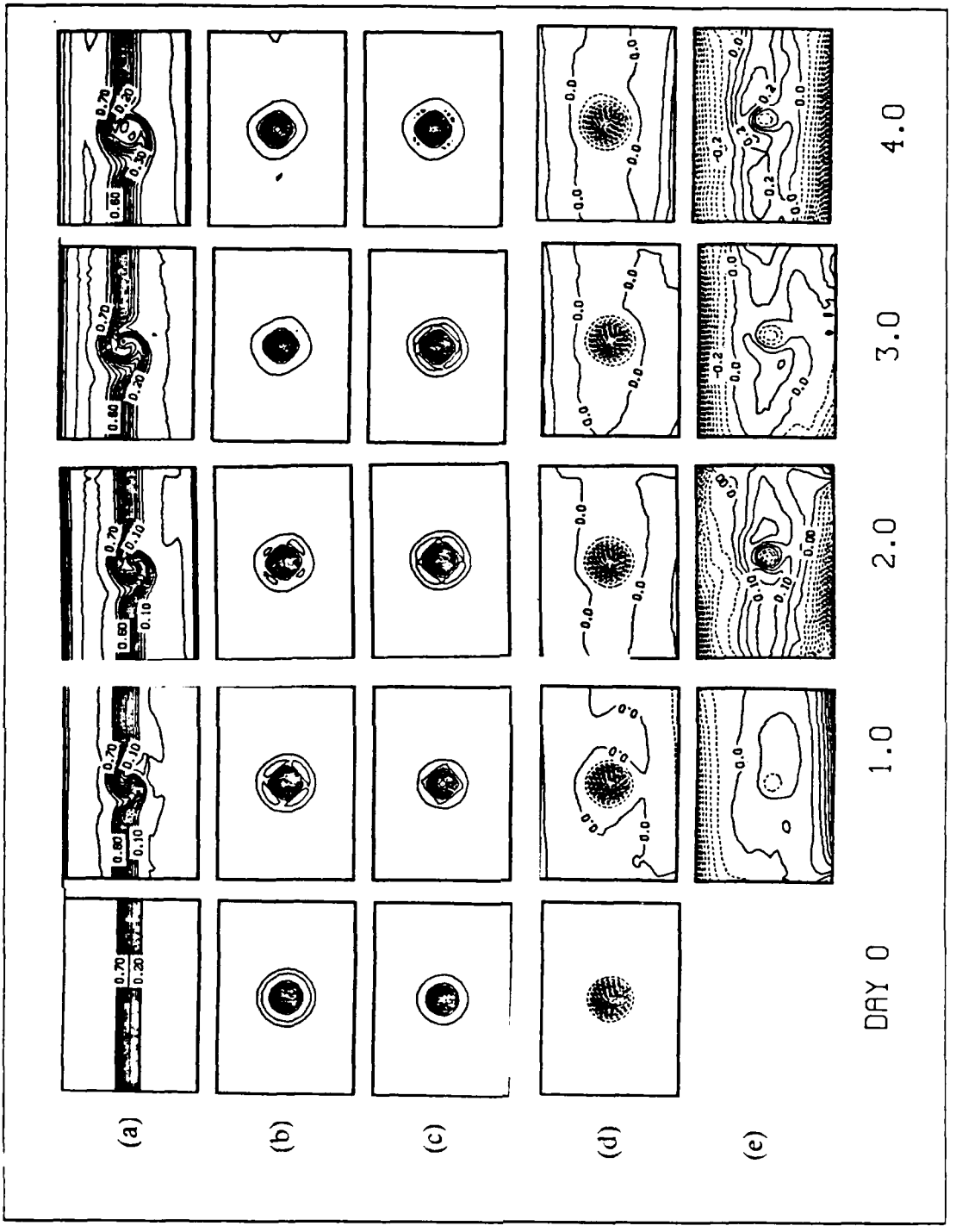

Figure 3.17 Experiment No. 6b (Cyclone, Daily 90° Shift to Light Off-Ice Winds).

Evolution of (a) ice concentration, (b) ocean upper layer potential vorticity, (c) ocean lower layer potential vorticity, (d) ocean surface height anomaly, and (e) ocean interface height anomaly. Contour interval for ice concentration is 0.05.

IV. DISCUSSION AND CONCLUSIONS

A. THE IMPORTANCE OF CYCLONIC EDDIES IN THE MIZ

Johannessen *et al.* (1987) found that most of the mesoscale eddies in the Marginal Ice Zone of the East Greenland Current were cyclonic in nature. Only 2 of the 15 eddies observed in Johannessen *et al.* (1987) were anticyclones. The authors hint that the two anticyclones may be the result of topography because these anticyclonic eddies were found only over topographic highs. The results of these simulations find that anticyclonic eddies interacting with an ice edge do not leave as clear of a signature of their presence at the ice edge. Simulated cyclonic eddies interacting with the ice edge leave their signature for much longer periods and, in some special circumstances, enhance the signature of the ocean eddy by aiding in concentrating the ice pattern over the eddy.

B. APPLICABILITY OF WIND SHIFT

The ice banding discussed by Häkkinen (1986a) was not observed as expected for two reasons:

1. The simulations in this study were not run out to the time for which ice banding was observed in Häkkinen (1986a).
2. The effects of ice banding could be masked by the interference caused by the ocean eddy.

Häkkinen (1986a) chose to vary winds sinusoidally with a period of four days to resemble the passage of atmospheric cyclones over the ice edge. This is an adequate approximation for the scale that Häkkinen (1986a) was simulating.

Shifting the winds 180° at intervals of 24 hours seemed to have little effect on the modeled ice pattern after a few days. However, the cases where the wind was shifted 90° developed very interesting ice patterns. The striking resemblance of these modeled ice patterns to those that have been observed in periods of moderate winds leads to the conclusion that the wind is extremely important in the development of these ice patterns in the MIZ.

C. NEAR-BREAK-AWAY ICE FORMATION

Another interesting result from the numerical simulations is that no simulated eddy ever broke completely away from the concentrated ice edge. There were some

cases where the concentration in the center of a cyclonic ice pattern was considerably greater than the ice concentration surrounding it, but not quite a complete separation. Thus, it can be concluded that the very interesting eddies observed during previous studies can not be explained merely by the existance of an eddy at the ice edge and by a regular pattern of wind shifts as used in this study. This suggests that the physical processes leading to a cut-off ice eddy are more complex than can be simulated in this study.

D. CONCLUSIONS

Observations indicate the presence of large (60 km) and mesoscale (5 to 10 km) eddies in the East Greenland Current Marginal Ice Zone. This study investigates the mesoscale eddy interaction with the ice edge. Previous model studies of ocean eddy interaction with the ice edge considered only strong (10 m s) and constant direction winds. This study is concerned with the periods where the wind speed is considered light and variable. The light winds and 24 hour interval wind shift are viable considerations because, as shown in Figure 1.2 and Figure 1.3, there are significant periods where the winds are light, and periods where the wind direction shifts several times over short periods. These short duration wind shift periods may be because of possible local atmospheric effects that are of a scale smaller than the circulation pattern considered by Häkkinen (1986a).

Smith *et al.* (1987) have shown the effect of eddies in the presence of no wind and in the case of strong constant direction (10 m s) winds and a broad ice band. The experiments completed here have verified the results of the no wind case for the cyclonic and anticyclonic eddies simulated by Smith *et al.* (1987) for a narrow marginal ice zone. Specifically, the experiments show that:

1. Three m s winds are too weak to induce upwelling or downwelling at the ice edge in less than of 6 days.
2. The effect of 3 m s winds on ice motion are comparable to the effect of 10 cm s ocean eddy motion.
3. Upwelling winds provide cyclonic vorticity to the ice field and, thus, augment cyclonic ocean-eddy-induced ice motion. Conversely, downwelling winds provide anticyclonic vorticity to the ice, countering cyclonic ocean-eddy-induced ice motion.
4. Cross-ice-edge motion is very sensitive to *magnitude* and *direction* of the wind, and the resulting signature of the ocean eddy in the ice is sensitive to cross-ice-edge motion.

5. Ice can become trapped over an ocean eddy, and can nearly break away from the ice edge as winds cause cross-ice-edge motion of the MIZ to the north.

6. Alternating upwelling downwelling 10 m s winds provide alternating cyclonic anticyclonic relative vorticity to the ice. If the period of reversal is short (24 hours) the spin-up spin-down effects cancel each other, leaving an ice edge signature comparable to no wind cases. If the duration is increased to 36 hours, the wind vorticity input dominates over the ocean vorticity input and the ice shows no eddy motion.

7. The near-break-away of ice from an ice edge occurs in these simulations only when significant wind induced cross-ice-edge motion causes the initial ice edge to retreat to the north, away from the ocean eddy leaving trapped ice over the eddy. This cross-ice-edge motion is sensitive to *magnitude*, *direction*, and *duration* of wind events.

E. RECOMMENDED FOLLOW-ON STUDIES

Because the region of the East Greenland Current has been observed to be the major source of heat exchange between the Atlantic water and arctic water, further studies should investigate the addition of thermodynamic effects on mesoscale eddies. Additionally, as anticyclones would melt ice, the response of ice to anticyclones and cyclones should show interesting differences.

APPENDIX
SYMBOLS AND NOTATION

A	Ice concentration	
A_0	Eddy maximum amplitude	
A_a	Laplacian lateral friction coefficient for ice concentration	
A_h	Laplacian lateral friction coefficient	
A_m	Laplacian lateral friction coefficient for ice mass	
β	Variation of Coriolis parameter with latitude	$= 3.8 \times 10^{-12} m^{-1} s^{-1}$
β_t	Topographic β	$= 3.2 \times 10^{-9}$
c_{ai}	Air-ice interfacial stress coefficient	$= 2.5 \times 10^{-3}$
c_{aw}	Air-water interfacial stress coefficient	$= 1.4 \times 10^{-3}$
c_{iw}	Ice-water interfacial stress coefficient	$= 7.5 \times 10^{-3}$
c	Phase speed of perturbation wave	
D	Ice thickness distribution	$= m\ \rho_i A$
Δx	Grid spatial resolution	= 1.0 km
Δt	Time increment	= 600 s
δ_{il}	Kronecker delta function	= 0 when i = 2
f_0	Coriolis parameter for mean latitude	$= 1.43 \times 10^{-4} s^{-1}$
g	Gravitational acceleration	$= 9.8\ m\ s^2$
g'	Reduced gravitational acceleration	$= g(\rho_2 - \rho_1)\ \rho_1$
γ	Nondimensional eddy size	$= L\ R_d$
H_1	Upper layer mean thickness	= 50 m
H_2	Lower layer mean thickness	= 4000m
h_i	Instantaneous layer thickness	= 50 m
L	e-folding scale of the ocean eddy	
m	Ice mass	
P_1	Pressure in the upper layer	$= g(h_1 + h_2 + d)$
P_2	Pressure in the lower layer	$= P_1 - g' h_1$
Q	Nondimensional eddy strength	$= v_{max}\ \beta R_d^2$
q_i	upper, lower layer potential vorticity	$= (f + \zeta_i) h_i$
R_d	First internal Rossby radius of deformation	$= [g' H_1 H_2\ f_0^2 (H_1 + H_2)]^{1/2}$
R_{0i}	Rossby number for upper(i = 1), lower(i = 2) layers	$= v_{max}\ fL$
ρ_a	Density of air	$= 1\ kg\ m^{-3}$

ρ_i	Density of ice	$= 910$ kg m^{-3}
τ^{ai}	Air-ice interfacial stress vector	
τ^{aw}	Air-water interfacial stress vector	
τ^{iw}	Ice-water interfacial stress vector	
t_{max}	duration of simulation	
u_w, v_w	Velocities in the x and y directions	
U_i, V_i	Transport in the x and y directions	
v_{max}	Open eddy maximum tangential velocity	$= 14$ cm s^{-1}
x,y	Cartesian coordinates directed NE and NW respectively	
ζ_i	Upper, lower layer relative vorticity	$= \nabla \times v_i$
∇	Gradient operator	$= \partial\ \partial x + \partial\ \partial y$
∇^2	Laplacian operator	$= \partial^2\ \partial x^2 + \partial^2\ \partial y^2$

LIST OF REFERENCES

Griffiths, R.W., and P.F. Linden, 1981: The Stability of Buoyancy Driven Currents, *Dyn. Atmos. Oceans*, **5**, 281-306.

Häkkinen, S. 1986a: Ice Banding in the Coupled Ice-Ocean, *J. Geophys. Res.*, **91**, 5047-5053.

_____, 1986b: Coupled Ice-Ocean Dynamics in the Marginal Ice Zones: Upwelling Downwelling and Eddy Generation. *J. Geophys. Res.*, **91**, 819-832.

Hurlburt, H.E., and J.D. Thompson, 1980: A Numerical Study of Loop Current Intrusions and Eddy Shedding. *J. Phys. Oceanogr.*, **9**, 1611-1651.

_____, and _____, 1982: The Dynamics of the Loop Current and Shed Eddies in a Numerical Model of the Gulf of Mexico. *Hydrodynamics of Semi-Enclosed Seas* Elsevier, 243-298.

Johannessen, J.A., O.M. Johannessen, E. Svendsen, R. Shuchman, T. Manley, W. Campbell, E. Josberger, S. Sandven, J.C. Gascard, T. Olaussen, K. Davidson, and J. Van Leer, 1987: Mesoscale Eddies in the Fram Strait Marginal Ice Zone During MIZEX 1983 and 1984. *J. Geophys. Res.*, **92**, 6754-6772.

Johannessen, O.M., J.A. Johannessen, J. Morison, B.A. Farrelly, and E.A. Svendsen, 1983: Oceanographic Conditions in the Marginal Ice Zone North of Svalbard in Early Fall, 1979 with Emphasis on Mesoscale Processes. *J. Geophys. Res.*, **88**, 2755-2769.

McWilliams, J.C., and G.R. Flierl, 1979: On the Evolution of Isolated Nonlinear Vortices. *J. Phys. Oceanogr.*, **9**, 1155-1182.

Mied, R.P., and G.J. Lindemann, 1979: The Propagation and Evolution of Cyclonic Gulf Stream Rings. *J. Phys. Oceanogr.*, **9**, 1183-1206.

Morison, J.H., M.G. McPhee, and G.A. Maykut, 1987: Boundary Layer, Upper Ocean, and Ice Observations in the Greenland Sea Marginal Ice Zone. *J. Phys. Oceanogr.*, **92**, 6987-7011.

Røed, L.P., and J.J. O'Brien, 1983: A Coupled Ice Ocean Model of Upwelling in the Marginal Ice Zone. *J. Geophys. Res.*, **88**, 2863-2872.

Smith, D.C. IV, A.A. Bird and W.P. Budgell, 1987: A Numerical Study of Mesoscale Ocean Eddy Interaction with a Marginal Ice Zone. Submitted to *J. Geophys. Res.*

_____, J.H. Morison, J.A. Johannessen, N. Untersteiner, 1984: Topographic Generation of an Eddy at the Edge of the East Greenland Current. *J. Geophys. Res.*, **89**, 8205-8208.

_____, and J.J. O'Brien, 1983: The Interaction of a Two-Layer Isolated Mesoscale Eddy with Topography. *J. Phys. Oceanogr.*, **13**, 1681-1697.

_____, and R.O. Reid, 1982: A Numerical Study of Nonfrictional Decay of Mesoscale Eddies. *J. Phys. Oceanogr.*, **12**, 244-255.

Wadhams, P., A.E. Gill and P.F. Linden, 1979: Transects by Submarine of the East Greenland Current. *Deep-Sea Res.*, **26A**, 1311-1327.

_____, and V.A. Squire, 1983: An Ice Water Vortex at the Edge of the East Greenland Current. *J. Geophys. Res.*, **88**, 2770-2780.

INITIAL DISTRIBUTION LIST

		No. Copies
1.	Defense Technical Information Center Cameron Station Alexandria, VA 22304-6145	2
2.	Library, Code 0142 Naval Postgraduate School Monterey, CA 93943-5002	2
3.	Chairman (Code 63Rd) Department of Meteorology Naval Postgraduate School Monterey, CA 93943	1
4.	Chairman (Code 68Co) Department of Oceanography Naval Postgraduate School Monterey, CA 93943	1
5.	Professor David C. Smith IV (Code 68Si) Department of Oceanography Naval Postgraduate School Monterey, CA 93943	3
6.	Professor A. J. Semtner (Code 68Se) Department of Oceanography Naval Postgraduate School Monterey, CA 93943	1
7.	Director Naval Oceanography Division Naval Observatory 34th and Massachusetts Avenue NW Washington, DC 20390	1
8.	Commander Naval Oceanography Command NSTL Station Bay St. Louis, MS 39522	1
9.	Commanding Officer Naval Oceanographic Office NSTL Station Bay St. Louis, MS 39522	1
10.	Commanding Officer Fleet Numerical Oceanography Center Monterey, CA 93943	1

11.	Commanding Officer Naval Ocean Research and Development Activity NSTL Station Bay St. Louis, MS 39522	1
12.	Commanding Officer Naval Environmental Prediction Research Facility Monterey, CA 93943	1
13.	Chairman, Oceanography Department U. S. Naval Academy Annapolis, MD 21402	1
14.	Chief of Naval Research 800 North Quincy Street Arlington, VA 22217	1
15.	Office of Naval Research (Code 420) Naval Ocean Research and Development Activity 800 North Quincy Street Arlington, VA 22217	1
16.	Scientific Liason Office Office of Naval Research Scripps Institution of Oceanography La Jolla, CA 92037	1
17.	Chief, Ocean Services Division National Oceanic and Atmospheric Administration 8060 Thirteenth Street Silver Spring MD 20910	1
18.	Professor R. Bourke,(Code 68Pa) Department of Oceanography Naval Postgraduate school Monterey, CA 93943-5002	1
19	Commanding Officer Naval Polar Oceanographic Center 4301 Suitland Rd Washington DC 20390	1
20.	Professor J. Q. Williams Physics Department Georgia Institute of Technology Atlanta, GA 30302	1
21.	LCDR Jeffrey L. Barker, USN 363 Prestonfield Lane Severna Park, MD 21146	3

END

DATE

FILMED

4-88

DTIC